UNIVERSITY OF COPENHAGEN

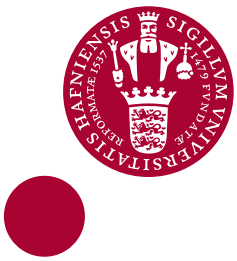

Phototrophic microbes form endolithic biofilms in ikaite tufa columns (SW Greenland)

Trampe, Erik Christian Løvbjerg; Castenholz, Richard W.; Larsen, Jens Erik Nybo; Kühl, Michael

Published in:
Environmental Microbiology

DOI:
10.1111/1462-2920.13940

Publication date:
2017

Document version
Peer reviewed version

Citation for published version (APA):
Trampe, E. C. L., Castenholz, R. W., Larsen, J. E. N., & Kühl, M. (2017). Phototrophic microbes form endolithic biofilms in ikaite tufa columns (SW Greenland). *Environmental Microbiology*, *19*(11), 4754–4770. https://doi.org/10.1111/1462-2920.13940

Download date: 08. Apr. 2020

Phototrophic microbes form endolithic biofilms in ikaite tufa columns (SW Greenland)

Erik Trampe[1], Richard W. Castenholz[2], Jens E. Larsen[1] and Michael Kühl[1,3]

[1]Marine Biological Section, University of Copenhagen, Strandpromenaden 5, DK-3000 Helsingør, Denmark

[2]Institute of Ecology and Evolution, University of Oregon, Eugene, OR-97403, USA

[3]Climate Change Cluster, University of Technology Sydney, Ultimo NSW 2007, Australia.

Running title: Phototrophic biofilms in ikaite

Keywords: Ikaite, microenvironment, variable chlorophyll fluorescence, light penetration, biofilm, cyanobacteria, diatoms.

Corresponding author: Name: Erik Trampe

Address: Strandpromenaden 5

3000 Helsingør, Denmark

Phone: +45 287 017 42

E-mail: etrampe@bio.ku.dk

Accepted Article

This article has been accepted for publication and undergone full peer review but has not been through the copyediting, typesetting, pagination and proofreading process which may lead to differences between this version and the Version of Record. Please cite this article as an 'Accepted Article', doi: 10.1111/1462-2920.13940

This article is protected by copyright. All rights reserved.

Accepted Article

Originality–Significance Statement: This study provides first details of the optical microenvironment and the spatial organization of endolithic microbial phototrophs within the porous ikaite crystal matrix of the conspicuous alkaline tufa columns only found in Ikka Fjord, Greenland. We provide a thorough description of a stratified microalgal and cyanobacterial biofilm that is embedded in polymeric substances in the outer layers of the ikaite matrix, and which may affect the tufa column formation. We further demonstrate that this endolithic biofilm serves as a substrate for grazing epifauna on the tufa columns.

Summary

Marine tufa-columns, formed by the hydrated carbonate mineral ikaite, present a unique alkaline microbial habitat only found in Ikka Fjord (SW-Greenland). The outermost parts of the ikaite columns exhibit a multitude of physico-chemical gradients, and the porous ikaite is colonized by endolithic phototrophic biofilms serving as a substrate for grazing epifauna, where scraping by sea urchins affects overall column-topography. We present a detailed study of the optical microenvironment, spatial organization, and photosynthetic activity of endolithic phototrophs within the porous ikaite crystal matrix. Cyanobacteria and diatoms formed distinctly colored zones and were closely associated with ikaite-crystals via excretion of exopolymers. Scalar-irradiance measurements showed strong attenuation of visible light (400-700nm), where only ~1% of incident irradiance remained at 20 mm depth. Transmission spectra showed in vivo absorption signatures of diatom and cyanobacterial photopigments, which were confirmed by HPLC-analysis. Variable-chlorophyll-fluorescence-imaging showed active photosynthesis with high-light acclimation in the outer diatom layer, and low-light acclimation in the underlying cyanobacterial part. Phototrophs in ikaite thus thrive in polymer-bound endolithic biofilms in a complex gradient microhabitat experiencing constant slow percolation of

This article is protected by copyright. All rights reserved.

Accepted Article

highly alkaline phosphate-enriched spring water mixing with cold seawater at the tufa-column-apex. We discuss the potential role of these biofilms in ikaite column formation.

This article is protected by copyright. All rights reserved.

Accepted Article

Introduction

The Ikka fjord in SW Greenland harbors a unique assemblage of underwater tufa columns composed of the hexa-hydrated carbonate mineral ikaite (Pauly, 1963; Buchardt *et al.*, 1997), which forms a porous matrix harboring a diverse assemblage of microbes (Stougaard *et al.*, 2002; Vester *et al.*, 2013; Glaring *et al.*, 2015). Hundreds of columns are situated in the innermost part of the Ikka fjord in Southwestern Greenland (Seaman and Buchardt, 2006), while ikaite column formation or larger solid ikaite assemblages have not been documented from other locations. The fjord is surrounded by steep ~500 m high Precambrian mountains of syenite and carbonatite (Emeleus, 1964) that play an important role in column formation. As meteoric water slowly percolates through the carbonatite layers, it is enriched with carbonate and phosphate and reaches a high alkalinity (pH >10). Strong hydraulic forcing leads the high pH water out under the fjord bottom, where it encounters cold seawater via seeps in the muddy seabed (Buchardt *et al.*, 1997, 2001). The mixing of water bodies leads to the chemical, non-biogenic formation and precipitation of metastable hexa-hydrated calcium carbonate crystals, i.e., ikaite ($CaCO_3 \cdot 6H_2O$). Ikaite is only stable at <6°C, and readily decomposes to calcite and water, when temperature rises above this threshold (Johnston *et al.*, 1916; Hume and Topley, 1926; Brooks *et al.*, 1950; Dickens and Brown, 1970). Originating as small chimneys on the seabed, the ikaite tufa columns can reach >20 m in height and several m in width. The tufa columns exhibit rapid potential growth rates at their apex reaching about 50 cm per year (Hansen *et al.*, 2011). While chemical formation of an ooze of ikaite crystals can easily be realized in the lab, it remains unknown how ikaite is deposited and cemented together forming tufa columns. However, it has been speculated that microbial formation of exopolymers could be important for the formation of the ikaite columns (Buchardt *et al.*, 2001). The tufa columns form a reef-like structure offering protection for juvenile fish and other marine organisms. The surface of the columns also appears as an important feeding ground for epifauna. High numbers of

This article is protected by copyright. All rights reserved.

various echinoderms, such as sea cucumbers, starfish, and sea urchins are observed on the ikaite columns, albeit their food source remains unknown.

The extreme physico-chemical conditions within the ikaite columns make them likely to harbor microbes concealing novel survival strategies and metabolic activities. The microbiology of ikaite tufa columns has been studied over several years, albeit with a strong focus on mapping the microbial diversity and obtaining bacterial cultures with biotechnological potential, e.g., bacteria harboring cold-active enzymes. These studies have mainly focused on heterotrophic bacteria, and sampling has often been done on more solid older parts of tufa columns at water depths with low light exposure (Stougaard *et al.*, 2002; Schmidt *et al.*, 2006a, 2007; Vester *et al.*, 2013, 2014). Stougaard *et al.* (2002) showed that these ikaite samples harbor a diverse microbial community of phototrophs (cyanobacteria, chlorophytes, and diatoms) and heterotrophs, where several novel bacterial species displayed low similarity with known 16S rRNA gene sequences from databases known at the time. Eukaryotic phylotypes based on 18S rRNA gene analysis also showed a low similarity to known database sequences. Four novel bacterial isolates from the tufa columns have been described in detail (Schmidt *et al.*, 2006b, Schmidt *et al.*, 2007, Schmidt *et al.*, 2010a, Schmidt *et al.*, 2010b). Kristiansen and Kristiansen (1999) isolated a new cryptophyte microalgal species, *Chroomonas ikaitensis*, from inside the ikaite matrix, and attributed blue-green patches in the ikaite to the presence of *C. ikaitensis*. However, the mentioned studies of microbial diversity relied on bulk sample analysis, and did not consider zonations of microbial populations in the ikaite microhabitat, nor did they include any measure of microbial activity in the tufa column matrix, and these important niche-defining aspects of the ikaite micro-habitat remain largely unexplored.

Recent amplicon sequencing studies of the microbial diversity in the apex of ikaite columns showed the presence of a phototrophic surface-associated community dominated by cyanobacteria (Glaring *et*

This article is protected by copyright. All rights reserved.

Accepted Article

al., 2015; Trampe *et al.*, 2016). The very first characterization of the *in situ* ikaite microenvironment was recently reported by Trampe *et al.* (2016), who demonstrated the presence of active photosynthesis by a mixed microalgal and cyanobacterial community inhabiting the ikaite column apex, which is a dynamic microhabitat characterized by steep O_2, pH and light gradients. In this study, we present a more detailed investigation of the structural organization, and zonation of endolithic phototrophs in the ikaite crystal matrix. We examine the prevailing light conditions, and photopigment composition in the ikaite columns and assess the photosynthetic activity and distribution of phototrophs in the ikaite crystal matrix. The potential role of microbial exopolymers for ikaite column formation by bonding of ikaite crystals is discussed, and our findings are synthesized in a conceptual model of the ikaite column microhabitat.

Results

Microstructure and microscopic analysis of the ikaite matrix.

Two apex samples from harvested ikaite columns showed well-defined green and yellowish bands in the outermost 1-3 cm of the ikaite, indicating the presence of an endolithic microbial community of phototrophs (Fig 1). The grey-white ikaite matrix at the tufa column apex was apparently recently formed, as judged by the presence of many >1 mm long sharp-edged ikaite crystals on the surface (Fig 1B). Column samples in refrigerated aquaria showed rapid ikaite precipitation in holes drilled for measurements; the holes became filled with new ikaite crystals within a few hours. Microscopic imaging of fresh ikaite samples revealed the presence of dense patches of mostly filamentous cyanobacteria (Fig. 1C) and pennate diatoms (Fig. 1D) that were embedded in transparent exopolymers (EPS) filling the ikaite crystal pore space (S-Fig. 1).

This article is protected by copyright. All rights reserved.

Confocal laser scanning microscopy (CLSM) confirmed a tight association between phototrophs, EPS, and ikaite crystals (Fig. 2, S-Fig 2), albeit the ikaite crystal structure was somewhat affected during the staining procedure, leading to more rounded crystals (Fig. 2E).

Scanning electron microscopy (SEM) showed the presence of collapsed exopolymers covering both ikaite crystals and microbes in the pore space (Fig. 3A), and demonstrated the presence of heterocystous cyanobacteria in close association with smaller bacterial cells directly attached to the cyanobacterial filaments (Fig. 3B).

Stratification of phototrophs in the ikaite tufa columns

Macroscopic imaging of photopigment fluorescence in a longitudinal cross-section through the apex of an ikaite tufa column showed the presence of two distinctly pigmented zones (Fig. 4A-D). Based on fluorescence induced by green light (515-560 nm) excitation of phycobiliproteins, we found that cyanobacteria inhabited a well-defined zone about 1-3 cm below the outer ikaite column surface (Fig. 4A). The diatom distribution was mapped via fluorescence induced by blue light excitation (450-492 nm) of Chl *c*, Chl *a* and Fucoxanthin, showing a patchy location of microalgae in the outermost 1 cm of the ikaite column, sometimes overlapping slightly with the outermost parts of the cyanobacterial zone (Fig. 4B). Despite some obvious patchiness due to structural heterogeneities in the ikaite matrix, the apex of tufa columns thus clearly exhibited the presence of a stratified phototrophic community harboring diatoms in the outermost and cyanobacteria in the innermost parts of a 1-3 cm thick zone below the surface of the ikaite column (Fig. 4C, D).

Pigment analysis and light penetration in the ikaite matrix.

This article is protected by copyright. All rights reserved.

Extraction and HPLC analysis of photopigments in bulk samples of the outermost 3 cm of the ikaite matrix confirmed the presence of both microalgal and cyanobacterial photopigments (Fig. 5, Table 1). Besides high levels of Chl *a* and the carotenoid, zeaxanthin, indicative of both microalgae and cyanobacteria, a minor amount of Chl *b* indicated the presence of chlorophytes and/or *Prochlorococcus*-like cyanobacteria, whereas the finding of the carotenoids fucoxanthin and diadinoxanthin indicated the presence of diatoms. The various forms of Chl *c* pigments characteristic of diatoms were not detectable with the HPLC method employed in this study.

Measurements of spectral scalar irradiance vs. depth in the ikaite matrix exhibited distinct absorption features, confirming the presence of several of the pigments identified in the HPLC analysis (Fig. 6). These spectra also demonstrated the presence of cyanobacterial phycobiliproteins, i.e., phycoerythrin (absorption peak at ~545 nm) and phycocyanin (absorption peak at ~620 nm), in the ikaite matrix; these water-soluble photopigments were not extracted in the HPLC analysis. The cyanobacterial phycocyanin absorption partly overlapped with the Chl *c* absorption (635 nm) of diatoms. Furthermore, a through in the scalar irradiance transmittance spectra near 800 nm indicated the presence of Bchl *a* indicative of the presence of anoxygenic phototrophic bacteria in the ikaite matrix, which was confirmed by the finding of small amounts of Bchl *a* in the HPLC analysis.

Light in the visible spectral range (400-700 nm) was most strongly attenuated in the ikaite, where only ~0.2-1% of the incident irradiance remained about 2 cm below the outer ikaite surface, whereas >10% of incident irradiance prevailed in the near infrared region of the spectrum (Fig. 6B). Scalar irradiance attenuation coefficients of photosynthetically active radiation (PAR, 400-700 nm) varied across different layers in the ikaite cross section (Fig. 6C): The outermost 0-6 mm of ikaite (0.15 mm^{-1}; r^2=1), the underlying highly pigmented diatom and cyanobacterial layer at 6-15 mm depth (0.31 mm^{-1}; r^2 = 0.997), the innermost edge of the cyanobacterial layer at 15-22 mm depth (=0.17 mm^{-1}; r^2=0.988), and

This article is protected by copyright. All rights reserved.

a layer of clean ikaite at 22-32 mm depth (0.04 mm^{-1}; $r^2 = 1$); r^2 values describe the goodness of a linear fit to ln-transformed scalar irradiance versus depth data over the given depth intervals. Measurements of the lateral light distribution around an incident red laser spot showed relatively high light propagation in the scattering ikaite matrix (Fig. 7), where ~50% of the vertically incident red laser light was detected about 2 mm from the laser spot, while ~10% remained at a distance of 10 mm.

Photosynthetic activity in the ikaite

Variable chlorophyll fluorescence imaging of ikaite cross-sections showed a well-defined pigmented zone with active photosynthesis (Fig. 8, 9). Macroscopic imaging showed chlorophyll fluorescence within the outermost 15 mm of the ikaite matrix, with highest fluorescence levels in a ~5 mm wide layer 5-10 mm below the ikaite surface (Fig. 8C, D). The green zone also exhibited the highest maxima in PSII quantum yields (Fig. 8E). Measurements of the effective PSII quantum yield during a sequence of rapidly increasing irradiance (10 s exposure to each irradiance step) enabled the calculation of rapid light curves (RLC) of relative PSII electron transport (rETR) vs. irradiance. While the effective quantum yields were similar across the endolithic zone (Fig. 8A), rETR values were highest in the most pigmented zone (Fig. 8B), reflecting a higher pigment density, and more efficient light capture than in the surrounding layers. The photon irradiance at onset of photosynthesis saturation, E_k, was calculated from curve fits to the experimental RLC data (averaged from three different areas of interest; AOI) and reached E_k values of 49.5 µmol photons m^{-2} s^{-1} in the central parts of the highly pigmented biofilm layer, and 47.2 and 51.1 µmol photons m^{-2} s^{-1} in the outer and innermost parts of the biofilm, respectively.

Microscopic imaging of individual cells in the pigmented ikaite layer indicated a difference between cyanobacteria and diatoms in their photosynthetic light acclimation (Fig. 9). Cyanobacteria (n=13),

This article is protected by copyright. All rights reserved.

displayed significantly lower values of E_k and $rETR_{max}$ than diatoms, (n=17); Means ±SE, $E_{k\text{-}cyano}$= 7 ± 0.2, $E_{k\text{-}dia}$ = 14 ± 0.9 (both in units of µmol photons m^{-2} s^{-1}), $rETR_{max\text{-}cyano}$ = 2.4 ± 0.2, and $rETR_{max\text{-}dia}$=3.4 ± 0.4. The cyanobacterial community showed an apparent downregulation or photoinhibition of PSII at photon irradiance levels >59 µmol photons m^{-2} s^{-1}, whereas diatoms did not show any signs of inhibition at photon irradiances up to 114 µmol photons m^{-2} s^{-1}, i.e., the maximal irradiance level used in the RLC measurements.

Discussion

This study presents novel insights to the spatial organization of microbial biomass, light microclimate, photosynthesis, and pigment composition of phototrophs in the active ikaite-depositing zone at the apex of the unique tufa columns in Ikka Fjord, SW Greenland. It also demonstrates that phototrophs inhabiting the tufa columns form dense biofilms anchored by EPS in the ikaite matrix.

Exopolymers in the ikaite matrix

Large and sharp-edged ikaite crystals were indicative of relatively freshly deposited ikaite at the growing column apex (Fig. 1), which formed a porous crystal matrix facilitating the diffuse outflow of alkaline spring water and mixing with seawater in the zones inhabited by phototrophic microbes. The structural microenvironment within the ikaite crystal matrix showed the presence of a stratified endolithic biofilm community of cyanobacteria and diatoms embedded in exopolymers (EPS), which cemented ikaite crystals and cells together (Fig. 2, 3; S-Fig. 1-2). While the staining procedures for CLSM apparently washed away some of the EPS (Fig. 2, S-Fig. 2), SEM images revealed a high amount of collapsed EPS formed during fixation and sample preparation, which formed an amorphous grainy coating on cells and ikaite crystals (Fig. 3).

This article is protected by copyright. All rights reserved.

Accepted Article

Accepted Article

It was previously speculated, that resilience to seawater exposure and extended lifetime of the ikaite crystals, even in older columns, could be attributed to microbial EPS formation shielding the highly soluble ikaite crystals (Buchardt *et al.*, 2001). Besides some preliminary observations in a recent study of the *in situ* microenvironment in the ikaite tufa columns (Trampe *et al.*, 2016), the present study is the first to clearly demonstrate abundant EPS in the phototrophic biofilms colonizing the outer layers of active ikaite formation zones. This lends further support to the hypothesis that EPS may contribute to column integrity, possibly even shaping column formation; however, more detailed studies of the types and role of EPS are needed.

The relative importance of abiotic and biotic mechanisms for tufa formation are still debated (e.g. Ford and Pedley, 1996). The reported high growth rates of the ikaite columns throughout the year (Hansen *et al.*, 2011), together with the extended periods of low light in the Ikka Fjord, rules out any noteworthy biogenic carbonate contribution to the column formation by phototrophs. However, EPS production by heterotrophic microorganisms could occur year round. Presently we can only speculate on the mechanisms by which EPS might modulate the ikaite matrix formation. It is well known that EPS slows down mass transfer in biofilms by impeding the diffusional exchange between the EPS-embedded cells and the surrounding medium (Decho, 1990; Flemming and Wingender, 2010). This leads to pronounced chemical gradients and dynamics in the biofilm microenvironment, e.g., light-driven changes between supersaturated and hypoxic conditions at day- and night-time, respectively (Kühl *et al.*, 1996). *In situ* microsensor measurements have shown pronounced O_2 dynamics in the apex of ikaite tufa columns (Trampe *et al.*, 2016), which was sometimes buffered by local accumulation of gas bubbles in the ikaite matrix. These O_2 dynamics and bubble formation would not be expected if the outermost ikaite matrix was simply percolated by an advective outflow of alkaline spring water. The presence of EPS-bound endolithic phototrophic biofilms can thus clearly change the

This article is protected by copyright. All rights reserved.

local ikaite microenvironment in response to photosynthetic and respiratory activity. Furthermore, EPS can exhibit selective binding of ions such as Ca^{2+} and can act as nucleation sites for carbonate precipitation (Riding, 2000), which can be modulated by local dynamics in saturation states due to photosynthetic activity, as shown in freshwater tufas (Shiraishi *et al.*, 2008).

Many other photosynthetic biofilm systems in the Arctic exhibit EPS production (Roeselers *et al.*, 2007; de los Rios *et al.*, 2015), which is thought to facilitate protection and/or survival during dark cold periods in the Arctic winter, especially in shallow habitats subject to freezing (e.g. Tashyreva and Elster, 2016). The ikaite tufa columns exhibit a constant flow of alkaline spring water, and ikaite forms throughout the winter months under a relatively constant temperature (Hansen *et al.*, 2011). The ikaite matrix is apparently not subject to freezing due to the more or less constant temperature of the flowing spring water (Hansen et al. 2011). However, the phototrophic communities in the tufa column apex will be strongly light-limited or in complete darkness during winter, where no new biomass production can be sustained by photosynthesis. How microbial activity in the tufa columns is fueled during winter is unknown. It has recently been shown that coastal microbial mat communities of cyanobacteria can reuse abundant EPS as a carbon source (Stuart *et al.*, 2016), and EPS formed by phototrophs could thus prove a key carbon source for heterotrophic microbial activity in the ikaite matrix, as has been shown for other biofilms (e.g. Taylor *et al.*, 2013). We speculate that breakdown of EPS might fuel microbial processes in the tufa columns during wintertime. Community compositions might also undergo drastic seasonal changes, where heterotrophic bacteria (and possibly heterotrophic processes in phototrophs) thrive on EPS and decaying parts of the phototrophic community during the dark winter months, while a bloom in the phototrophic organisms and net carbon fixation occur during summer months. With the apparent column growth throughout the year (Hansen et al. 2011), the EPS will have to be abundant throughout as well, and thus the EPS might shift from being of phototrophic to heterotrophic origin.

This article is protected by copyright. All rights reserved.

However, comparative investigations of EPS, and microbial diversity changes in the tufa columns between summer and winter are needed to further elucidate the potential role of EPS as a substrate.

Dominant phototrophic groups

Marker pigments are often used to identify major functional groups of phototrophs, (Everitt *et al.*, 1990; Barlow *et al.*, 1993; Zapata *et al.*, 2000; Jeffrey *et al.*, 2011), and our microscopic observations of dominant phototrophs in the ikaite were further supported by HPLC pigment analysis (Fig. 5, Table 1) showing predominance of cyanobacteria and diatoms, but also a minor presence of green algae (Chlorophyceae) or *Prochlorococcus*-like cyanobacteria and Bchl *a*-containing purple anoxygenic phototrophs. In line with Trampe *et al.* (2016), who showed the presence of active phototrophs within the ikaite column apex, we found a distinct zonation of phototrophs with pennate diatoms predominating in the outermost cm's of the ikaite matrix, while cyanobacteria formed a distinct green layer below the diatom zone ~1-2 cm below the outer ikaite surface. The cyanobacterial layer was predominated by filamentous morphotypes, some with heterocysts (Fig. 3) indicating a potential for N_2-fixation in the ikaite crystal matrix. We speculate, that combined nitrogen may be a major limiting nutrient in the ikaite matrix, where phosphate-enriched alkaline spring water is mixed with seawater. Scalar irradiance measurements showed strong light attenuation in the ikaite crystal matrix, with distinct changes in the spectral light composition with depth (Fig. 6). The cyanobacteria, as indicated by absorption signatures of phycobiliproteins in the scalar irradiance spectra, dominated in the innermost parts of the pigmented zone. *In vivo* spectral signatures of the pigment fucoxanthin showed the presence of diatoms in the outermost pigmented layer, where HPLC analysis confirmed the presence of fucoxanthin along with another diatom carotenoid, diadinoxanthin. Diadinoxanthin is a photoprotective carotenoid, which can be converted to diatoxanthin upon high light exposure leading to

This article is protected by copyright. All rights reserved.

Accepted Article

quenching of radiative stress (Brunet *et al.*, 1993). The apparent absence of diatoxanthin in the analyzed ikaite samples indicates that the diatom biofilm thrives in a low-light habitat governed by the steep light attenuation in the outermost ikaite layers. Small amounts of Chl *b* were also evident in the HPLC analysis, indicating the presence of green algae or *Prochlorococcus*-like cyanobacteria, but we could not assign these pigments to particular morphotypes, and cyanobacteria and diatoms were the predominant phototrophs in the ikaite matrix.

The finding of spectral signatures and trace amounts of Bchl *a* in the bulk ikaite sample analysis (Table 1, Fig. 6) also indicate that anoxygenic phototrophs may occur in the tufa columns, probably benefitting the efficient penetration of near infrared radiation (NIR) into deeper layers of the ikaite matrix, though the efficient absorption of NIR in seawater would confine this spectral niche to the tufa column apex. Our microscopic investigations also showed the presence of other microorganisms associated with cyanobacteria, ikaite crystals, and in the collapsed EPS matrix, in line with earlier findings of diverse bacterial OTUs across the different zonations of phototrophs in the ikaite column apex (Trampe et al. 2016).

Besides the isolation of a microalgal cryptophyte (Kristiansen and Kristiansen, 1999), cultivation of microbes from the ikaite columns have to this point focused on the heterotrophic community, where Schmidt el al. (2006a) characterized >200 bacterial isolates with respect to pH and temperature tolerance. Most isolates were psychrotrophic and alkalophilic, with a large fraction growing only in media of pH 10. Several isolates have a strong potential for industrial and biotechnological application, e.g., the Gram-positive bacterium *A. ikkense* harboring a low temperature β- galactosidase displaying >60% activity at 0°C (Schmidt *et al.*, 2010a). In contrast, enrichment and cultivation of phototrophs from the ikaite columns has just begun, and we are presently characterizing several cyanobacterial and

This article is protected by copyright. All rights reserved.

diatom isolates, where EPS formation is common (Trampe *et al.*, unpublished data).

Physico-chemical microenvironment

The ikaite tufa columns harbor internal flow channels that guide lower density meteoric water to the column apex, where it is mixed with seawater. This leading to ikaite formation and upward column growth that is only limited by the thermo- and chemo-cline in the uppermost water column during summer and mechanical ice scouring during winter (Hansen *et al.*, 2011). The diffuse outflow of tufa column pore-water at the apex creates a mixing zone with seawater in the outer ikaite crystal matrix of the columns (Hansen *et al.*, 2011). This leads to the formation of physico-chemical gradients through the ikaite matrix from the innermost flow channels and across the two distinct phototrophic layers towards the tufa column surface. Trampe *et al.* (2016) showed a constant pH gradient ranging from pH 10 below the ~1-2 cm thick phototrophic zone to ~pH 9 at the tufa column surface irrespective of changes in ambient irradiance and measurement location on the column apex. This is expected in presence of a constant diffuse outflow of spring water and thus a relatively slow mixing with seawater in the outermost tufa column layers. The observed zonation of phototrophs could indeed be governed by the pH and/or salinity gradient across the observed growth zones. For the phototrophic community to cope with these microenvironmental changes in physico-chemical conditions, it requires either motility and/or metabolic plasticity (Bergman *et al.*, 2008). Cyanobacteria generally tolerate more alkaline conditions (pH 8-10) than diatoms (Brock, 1973; Goldman *et al.*, 1982; Kupriyanova *et al.*, 2007).

While pH could be a prime determinant of the overall phototroph zonation in the ikaite matrix, the relatively distinct growth zones could also be governed by light attenuation (Fig. 6, 10). Maximal *in situ* levels of incident photon irradiance (400-700 nm) at the tufa column apex were ~450 µmol

This article is protected by copyright. All rights reserved.

photons m^{-2} s^{-1} on a clear day in August, (Trampe *et al.*, 2016), and this irradiance would be close to the maximal light level reaching the surface of the sampled columns. Using our light attenuation data, phototrophs about 20 mm inside the ikaite matrix would receive only ~5.2 µmol photons m^{-2} s^{-1} of light during peak hours of the summer months (Fig 6C).

Light incident on the ikaite columns may be rather directional under different sun angles, yet the macroscopic fluorescence imaging showed a relative homogenous banding of pigmented zones over the column apex (Fig. 4). As the ikaite matrix showed a potential for efficient lateral spreading of light due to scattering in the crystal matrix (Fig. 7), we speculate that the ikaite crystal matrix may enable some degree of lateral homogenization of the light field in the outer parts of the ikaite column, which could facilitate a more even exposure and zonation of the endolithic phototrophs. A similar effect has been demonstrated in symbiont-bearing corals (Wangpraseurt *et al*., 2014), but more detailed studies of the optical properties of ikaite are necessary. We also note that our measurements of lateral light spread were limited to a narrow spectral range (647-658 nm), that overlapped only to a small degree with the absorption spectrum of the major photopigments in the ikaite matrix.

In many microbial mats and biofilms, high-light tolerant diatoms typically thrive above a dense cyanobacterial layer exhibiting low-light acclimation (Lassen *et al*., 1992; Decho 2000; Wieland and Kühl, 2000). Furthermore, both diatoms and cyanobacteria in such systems often exhibit motility patterns enabling them to adjust their vertical position for optimal light exposure during daytime (Garcia-Pichel *et al*., 1994; Kruschel and Castenholz, 1998; Serôdio *et al*., 1997; Ezequiel *et al*., 2015). While motile filaments dominated the cyanobacterial layer, the diatom layer showed very little cell motility. Preliminary observations of small ikaite samples kept under low light showed a visible greening of the ikaite surface over time (data not shown), indicating that motility may enable the cyanobacteria to position themselves into more optimal light conditions under low light regimes or,

This article is protected by copyright. All rights reserved.

e.g., upon extensive crystallization of ikaite in outer layers of the column creating a decrease in local irradiance over time.

The layering and overall distribution of phototrophs in the ikaite columns was also affected by grazing sea urchins (Supp. Fig. 3). On tufa columns with many sea urchins, small intrusions or paths of movement were carved into the ikaite by the sea urchins. Ikaite pellets were observed to be discharged by the grazing sea urchins (Supp. Fig. 3), and in some cases the surrounding seabed was covered in small whitish pellets around the base of heavily populated columns. Grazing seemed to be limited to the outermost, newly precipitated ikaite, presumably very rich in microorganisms and EPS, while motile phototrophs retracting to deeper layers may be less affected by this grazing pressure.

In situ measurements of O_2 concentration profiles, and variable chlorophyll fluorescence showed active photosynthesis in the intact tufa column apex (Trampe *et al.*, 2016). In this study, we investigated the photosynthetic capacity of the endolithic biofilm community within the outermost 2 cm of the ikaite matrix at higher spatial resolution (Fig. 8, 9). We found a clear zonation in pigmentation (Fig. 8A) and chlorophyll fluorescence yield (Fig. 8B), although photosynthetic capacity showed an almost identical yield in PSII activity across the different zones (Fig. 8C). However, there were apparent differences in how relative electron transport related to PSII activity (*rETR*) changed with irradiance in the diatom and cyanobacterial zone (Fig. 8D, 9), where diatoms exhibited more efficient photosynthesis with a higher E_k and significantly higher $rETR_{max}$ as compared to the cyanobacteria. Diatoms were thus apparently acclimated to higher light levels than the cyanobacteria, explaining the predominance of cyanobacteria in the lower irradiance regime below the diatom layer. Values used for calculating the rETR vs. irradiance curves of different zones in Figure 8 were averaged over several areas of interest (AOI) and thus represent averages of many cells within each zone with no distinction between diatom and cyanobacterial

This article is protected by copyright. All rights reserved.

contributions to the measured signal within the AOI's. The *in situ* study of Trampe *et al.* (2016) also found relatively low E_k values similar to those measured for cyanobacteria and diatoms in the present study. The Ikka fjord is covered with ice during winter, and the sun is at a very low angle, literally rendering the interior of the tufa columns dark. At winter solstice, the sun rises around 9:00, setting again behind the mountains around 13:00 with a maximum altitude of 6°, which allows only 4h of direct sunlight, most of which is reflected by the snow-covered sea ice (www.sunearthtools.com). Therefore, during winter, there would be essentially no light available for photosynthesis in the ikaite matrix. Some oxygenic phototrophs can sustain life with an extreme reduction in their metabolism, and bring respiration to a minimum entering a quasi-dormant state. Nymark *et al.* (2013) found a rapid re-illumination acclimation of the diatom *Phaeodactylum tricornutum* that maintained a functional photosynthetic apparatus during darkness although fundamental transcriptional, metabolic, and intracellular changes occurred in the dark period, i.e., by down-regulating genes encoding for enzymes in the Chl *a* synthesis pathway. Other means of survival could involve the formation of cysts or spores by diatoms or akinetes by a few types of cyanobacteria (Stambler and Dubinsky, 2007). Formation of resting stages has been documented for an Antarctic lake experiencing sub-zero temperatures (Singh and Elster, 2007), and Vincent *et al.* (1993) reported that cyanobacteria and diatoms survived the winter period under complete darkness in Antarctic fresh water ponds. However, further *in situ* sampling is necessary to resolve the metabolic status of the phototrophic community, especially during winter.

In conclusion, this first description of the ikaite tufa column microhabitat demonstrated the presence of an endolithic biofilm community in the outermost 1-2 cm of the freshly deposited ikaite matrix, at the tufa column apex. The biofilm community was stratified into an outer diatom-dominated layer on top

This article is protected by copyright. All rights reserved.

Accepted Article

of a cyanobacterial layer, both exhibiting pronounced formation of EPS. These endolithic biofilms thrive in a unique microbial habitat that is characterized by a multitude of physical, and chemical gradients as illustrated in Figure 10, where we have summarized experimental findings from the present study and the *in-situ* study of Trampe et al. (2016) into a conceptual model. We present strong indications that the microbial community interacts with the chemical ikaite crystal formation, where the "cementing" properties of the EPS might influence the shaping of the overall tufa column matrix. However, further *in situ* investigations in combination with molecular genetics and culture based analysis of the phototrophic community, as well as a deeper understanding of the characteristics and regulation of EPS production, are necessary to unravel the role of microbes in tufa column formation. Besides studies of microbial growth plasticity in terms of temperature, pH, and low/high light tolerances, laboratory studies of artificial ikaite precipitation in specific cultures of phototrophs from the tufa columns could further elucidate microscale interaction between phototrophs, EPS, and column formation. Isolation and cultivation of ikaite phototrophs could also yield novel strains with specialized metabolic survival mechanisms optimized to the unique microenvironment within the tufa columns. Culturing experiments combined with *in-situ* investigations of the photosynthetic and respiratory activity throughout the year, i.e., under various light and ambient seawater temperature conditions could further contribute to the understanding of how ikaite phototrophs cope with extended periods of no or very low photon flux.

Experimental Procedures

Sampling and transportation of samples

This article is protected by copyright. All rights reserved.

The investigated ikaite tufa columns belong to a range of columns branching from a NNE-oriented ridge forming part of the base of one of the most massive ikaite formations ("The Atoll") in Ikka Fjord, SW Greenland (61°11.635'N 048°01.434'W) (Fig. 1A). A more detailed account of the sampling site and *in situ* characteristics of the ikaite column habitat are given elsewhere (Trampe *et al.*, 2016). In August 2013, the uppermost 30 cm (apex) of two ikaite columns were sawed off by a certified commercial scuba diver at a depth of 7 m below mean sea level. The tufa column apex samples were bagged and immersed in a mixture of seawater and spring water escaping the columns at the sampling depth. The samples were transported to a field laboratory, where they were kept in darkness and refrigerated seawater at ~4°C prior to transport to the nearby Danish Naval Station "Grønnedal" (61°13.974'N 048° 05.775'W). Laboratory investigations in Grønnedal commenced within 24 hours after the *in situ* sampling. Columns showed no sign of dehydration of calcium carbonate or other compression of crystals from external factors, such as grazing by sea urchins. For subsampling, the two column pieces were carefully cut with a fine handsaw while immersed in an aquarium filled with the mixed *in-situ* water. This sectioning yielded two different cross sections: i) a longitudinal section cut through the middle of the vertical axis of the first piece, splitting the apex part in half vertically (Fig. 4C), and ii) a horizontal section cut approximately 15 cm from the top of the second column apex sample (Fig. 6-7). Prior to experiments, the cut ikaite pieces were then placed at 4°C in a temperature-controlled aquarium filled with the mixed *in-situ* water collected at the sampling depth.

Samples were air transported to Denmark five days after sampling for the remaining analysis. During transportation, all samples were kept immersed in cold (1-5°C) *in-situ* water. Microscopic assessments of the photosynthetic performance of individual cells in the ikaite matrix were performed immediately upon arrival to Denmark.

This article is protected by copyright. All rights reserved.

Macroscopic fluorescence imaging

The overall distribution of phototrophs was investigated by macroscopic fluorescence imaging of a longitudinal cross section through the apex of an ikaite column (Fig. 4). Fluorescence images were recorded, while the immersed ikaite sample was illuminated with a fiber-optic halogen lamp (Schott KL 2500 LCD, Schott GmbH, Germany), which was equipped with a collimating lens set to evenly illuminate the entire section of ikaite. The lamp was fitted with a blue or a green excitation filter (Blue: FITCA-40, 450-492nm, Green: FITCE-45, 515-560nm, Schott GmbH, Germany), which were placed sequentially in the light path. Autofluorescence of the phototrophs was recorded with a digital SLR camera and lens (EOS 7D digital SLR camera, and EF 24-70mm f/2.8 L USM lens, CANON Europe Ltd., Middlesex, UK). The CCD-chip in the camera only exhibits sensitivity to light in the spectral range of ~400-680 nm (Sigernes *et al*., 2009), and as the camera was fitted with a long-pass emission filter (RG 645, Schott GmbH, Germany) it was possible to record detailed images of pigment autofluorescence of the phototrophs in the 645-680 nm spectral range. The autofluorescence properties of ikaite and potentially other carbonate minerals present in the tufa column matrix are not known. However, fluorescence emission below ~700 nm was not observed in samples when exited in the spectral ranges used here, i.e., 450-492 nm and 515-560 nm (Smith *et al*. 2014), and interferences between carbonate and photopigment fluorescence were thus not observed. Obvious "false signal" due to reflectances from the aquarium glass and metal stands holding the ikaite column in place, were deleted from the original Canon RAW fluorescence images recorded under blue and green excitation. Then the images were optimized by thresholding low pixel values, and enhancing the contrast for the remaining pixels. The fluorescence images were then assigned false colors: cyan (representing the fluorescence of cyanobacterial phycoerythrin, exited by 515-560 nm light), and red (representing fluorescence of diatom Chl *c*, Fucoxanthin, and to some degree Chl *a*, exited by 450-492 nm light).

This article is protected by copyright. All rights reserved.

The false color images were superimposed in Adobe Photoshop CC (Adobe Systems Incorporated, California, USA).

Microscopic image and video acquisition

A digital USB microscope camera (AM7013MZT, Dino-Lite; AnMo Electronics Corp, Taiwan) was used to obtain microscopic images and video recordings of ikaite crystals, and of the green and brown pigmented zones within the ikaite matrix. For this, a freshly sampled ikaite column was broken into fragments of ~1 cm^3 that were kept moist at 6°C in a Petri dish with *in-situ* spring water during image acquisition.

Confocal laser scanning microscopy

A cohesive ikaite crystal matrix sample (~1 mm^2) from a yellow-greenish area representing overlapping zones dominated by both cyanobacteria and diatoms was placed on a microscope slide with a coverslip sealed on two opposing sides to create a directional flow channel across the sample. For staining of EPS, a solution of the fluorescent TRITC lectin (#L5264, Sigma-Aldrich Chemie GmbH, Munich, Germany; 100 µg per mL of filtered Ikka spring water) was continuously provided as droplets to the front of the cover slip, while dragging the flow from the opposite end of the flow channel with filter paper. By this method, the solution was effectively percolated into the sample before incubation on ice for two hours. Thereafter, a lectin rinse and $CaCO_3$ staining procedure was done in the same manner by carefully percolating the mounted samples with a calcein solution (C0875, Sigma-Aldrich Chemie Gmbh, Munich, Germany; 200 µg per L of filtered Ikka spring water) that simultaneously removed any unbound lectins and stained the $CaCO_3$. This staining/rinsing step was

This article is protected by copyright. All rights reserved.

repeated three times, where after samples were soaked in the calcein solution at 4°C for 12 h. Finally, the samples were percolated with pure filtered Ikka spring water and mounted in Vectashield antifade mounting medium with DAPI (Vector Laboratories, Burlingame, CA) prior to storage at -20°C. The stained ikaite samples were imaged on an Olympus FluoView FV1000 confocal laser scanning microscope, where confocal image stacks were recorded in steps of 5 µm. Phototrophs were imaged via their autofluorescence in the far-red channel (diatoms; excitation with 635 nm, emission 650 to 800 nm) and in the red channel (cyanobacteria; excitation with 543 nm, emission 585-625 nm). DNA was identified by DAPI fluorescence recorded in the blue-green channel (excitation with 405 nm, maximum emission 461 nm). The calcein-stained ikaite crystals were imaged with excitation at 488 nm and an emission maximum at 509 nm, and were additionally visualized by transmitted light images. The fluorescence of lectin-stained EPS was detected in the green channel (excitation with 488 nm, emission 500 to 550 nm). Imaris 7.0 (Bitplane AG, Zu□rich, Switzerland) was used for image analysis and adjustment of brightness and contrast of the respective channels using the tool "*Image adjustment*". Furthermore, the software was used to create isosurfaces of the ikaite crystals based on the DAPI-signal (or the absence thereof) using the "*Surface*"-tool. Subsequently, maximum projections and rendering of Z-stacks into 3D/2D images as well as video clips were acquired by the software tools "*Snapshot*" and "*Video*".

Scanning electron microscopy

Scanning electron microscopy (SEM) analysis was performed on ikaite samples with visible phototrophs. Small pieces of ikaite (~5 mm^3) were submerged in 2% glutaraldehyde in 0.05 M phosphate buffer solution (pH 7.2) immediately after sampling and were kept at 4°C until further

This article is protected by copyright. All rights reserved.

processing. Samples were then post-fixed in 1% osmium tetroxide with 1.5% potassium ferrocyanide (Knott *et al.*, 2008) and embedded in Epon according to standard procedures (Hayat, 2000). Subsequently, samples were sputter coated with gold (SEM coating unit E5000; Polaron) and imaged with a dual-beam high resolution SEM system (Quanta FEG 3D, FEI Europe, Eindhoven, The Netherlands). Images were colored in false colors in Adobe Photoshop 2015 CC (Adobe Systems Incorporated, California, USA) to highlight specific features.

Photopigment analysis

Ikaite samples were analyzed for their photopigment content with high-pressure liquid chromatography (HPLC) using a method slightly modified from Frigaard *et al.* (1996). Fresh samples of the outermost ~3 cm thick ikaite layer were frozen at -20°C in the field and were kept at this temperature for 6 days during transportation to Denmark, where the samples were then stored at -80°C until pigment extraction was done. Each of three small homogenized subsamples (~1.5 g) from the pigmented ikaite zone was mixed with 1.5 mL sterile filtered water (T=18°C, pH=7.2) and vortexed for 1 min until the ikaite crystals were completely dissolved. The mixture was then centrifuged at ~10,000 g for 5 min, and the supernatant was removed. The remaining pellet was re-suspended for pigment extraction in 0.4 mL of an acetone-methanol (7:2, vol/vol) mixture (T=4°C) and sonicated using an ultrasonicator (Misonix 4000, Qsonica LLC., Newtown, CT, USA) under dim light for 20 s. The sonicated cells were then extracted in darkness on ice for 2 min. The extracts were briefly centrifuged to pellet cell debris, and the supernatants were mixed with 15 µL ammonium acetate (1 M) in 0.3 mL HPLC vials. A 100 µL sample of the mixture was then immediately injected into the HPLC system. The injected pigment extract was separated and analyzed by a diode array detector connected to the HPLC system (HPLC-DAD & Agilent 1260 Infinity, Agilent Technologies, Santa Clara, CA, USA fitted with a Novapak C18

This article is protected by copyright. All rights reserved.

Accepted Article

column; dimensions: 3.9 x 300 mm) detecting spectral absorption of the eluents. The extracts were run at a column temperature of 30°C for 69 min. The extracts moved with a flow-rate of 1.0 mL min^{-1} in solvent A (methanol:acetonitrile:water, 42:33:25, vol/vol/vol), and solvent B (methanol:acetonitrile:ethyl acetate, 50:20:30, vol/vol/vol). In the separation process, the mobile phase changed linearly from 30% solvent B at the time of injection to 100% after 52 min, before staying at 100% for 15 min and then falling back to 30% within 2 min. Pigments were identified manually from their HPLC chromatogram of retention times and spectral signatures of absorption maxima (Fig. 5, Table 1) using the HPLC control software (OpenLAB CDS ChemStation Edition, Agilent Technologies, Santa Clara, CA, USA) and by comparison to relevant literature (Everitt, 1990; Hoff and Amesz, 1991; Frigaard *et al.*, 1996; Zapata *et al.*, 2000).

Variable chlorophyll fluorescence imaging

We used pulse-amplitude-modulated variable chlorophyll fluorescence imaging (Imaging-PAM) (Schreiber *et al.*, 1994; Schreiber, 2004; Kühl and Polerecky, 2008) to assess the photosynthetic performance in fresh ikaite column samples. We employed macroscopic imaging from the surface to a depth of ~2 cm inside the ikaite column in combination with microscopic imaging revealing the photosynthetic capacity of individual cells embedded in aggregates of EPS and ikaite crystals. Macroscopic imaging was done with a red light measuring head (620 nm), (IMAG-MIN/R; Heintz Walz GmbH, Germany). The system was calibrated using a light meter connected to a cosine-corrected mini quantum PAR sensor (ULM-500, MQS-B, Walz GmbH, Germany). During measurements, a cross-section of intact ikaite was placed in a Petri dish containing a mix of seawater and Ikka-spring water keeping the ikaite completely water saturated at a temperature of 3-5°C.

This article is protected by copyright. All rights reserved.

Microscopic imaging of the photosynthetic performance of individual cyanobacteria and diatoms was done with a microscope version of the Imaging-PAM system described above with the addition of a Red-Green-Blue (RGB) LED excitation lamp (IMAG-RGB; Heinz Walz GmbH, Effeltrich Germany). The microscopy PAM system is described in detail elsewhere (Trampe *et al.*, 2011). The RGB LED enabled us to discriminate between different functional groups of phototrophs by deconvolution of fluorescence images from different pigment signatures (see details in Trampe *et al.*, 2011). Briefly, this was done by detecting differences in the maximal chlorophyll fluorescence yield of cyanobacteria and diatoms when exited by red (λ_{max}: 622 nm, half bandwidth (HBW): ~65nm), green (λ_{max}: 520nm, HBW: ~90 nm), and blue (λ_{max}: 460nm, HBW: ~80 nm) measuring light. The phototrophs absorb the measuring light according to their pigment composition, with cyanobacteria showing a high fluorescence yield from red light absorption by their phycobiliproteins, while diatoms show a higher yield under blue and green light due to their chlorophylls and the carotenoid fucoxanthin (see more details in Trampe *et al*. 2011). For the variable chlorophyll fluorescence microscopy, subsamples of ikaite were carefully homogenized on microscope slides before imaging. The slides were placed in a custom temperature-controlled slide holder, keeping the sample temperature at 4°C during measurements (Trampe *et al.*, 2011). The system was fitted with a 20x high-numerical-aperture objective (20x/0.8, Plan-Apochromat, Carl Zeiss GmbH, Germany).

For both macro- and micro-scopic measurements, the samples were allowed to dark adapt for 15 min before onset of measurements. In the dark-adapted state, all reactions centers of PSII were open and the minimal fluorescence yield (F_0) was imagined with weak, non-actinic modulated measuring light. During application of a high-intensity saturation pulse, all PSII reaction centers close allowing imaging

This article is protected by copyright. All rights reserved.

of the maximal fluorescence yield (F_m) over the ikaite sample. From these data, images of maximum PSII quantum yield could be calculated as in Schreiber (2004):

$$F_V/F_m = (F_m - F_0)/F_m \quad (1)$$

Correspondingly, based on imaging of the fluorescence yield, F, under illumination of the sample with a predefined level of actinic light (PAR, in µmol photons m^{-2} s^{-1}), and the maximum fluorescence yield, F_m', measured under a following saturation pulse, images of the effective PSII quantum yield could be calculated as:

$$\Phi_{PSII} = (F_m' - F)/F_m' \quad (2)$$

From these values, the relative photosynthetic electron transport rate (*rETR*), could be derived using the following equation:

$$rETR = \Phi_{PSII} \times \mathrm{PAR} \times \mathrm{K} \quad (3)$$

where PAR is the incident quantum irradiance and K is a constant set to be 0.5 assuming an equal charge separation between photosystem II and I. The light saturation coefficient, i.e., the photon irradiance at onset of light saturation of photosynthesis, E_k was calculated as $E_k = rETR_{max}/\alpha$, where $rETR_{max}$ is the maximum activity and α is the initial slope of the *rETR* vs. photon irradiance curve; both parameters were obtained by curve fitting of *rETR* vs. photon irradiance curves with an exponential function (Webb *et al.*, 1974) using a non-linear Levenberg-Marquardt fitting algorithm (OriginPro 2015, OriginLab Corporation, Northampton, MA, USA).

Spectral scalar irradiance

Spectral scalar irradiance was measured as a function of depth in a cross-section of an intact ikaite column sample by inserting a fiber-optic mini probe, (US-SQS/L Submersible Spherical Micro

This article is protected by copyright. All rights reserved.

Quantum Sensor, Walz GmbH, Germany) into holes (10 mm deep, ~3 mm wide) that were carefully drilled into the ikaite matrix. Measurements were conducted from the center of the ikaite sample and outwards to the outer sample surface, drilling the holes one at a time before measuring, keeping an intact light path in the ikaite between sensor and the light source for each distance measurement. The ikaite column sample surface was illuminated from the side with a fiber-optic halogen lamp (Schott KL 2500 LCD, Schott GmbH, Germany) placed 20 cm from the aquarium, providing an even illumination over the area of interest. Spectral scalar irradiance was recorded in each hole with the mini probe connected to a PC-controlled spectrometer (USB2000+, Ocean Optics Dunedin, Florida, USA). All measurements were corrected for electronic dark noise, and were normalized to the incident spectral irradiance at the ikaite surface (Fig 6).

The vertical diffuse attenuation coefficient of the photon scalar irradiance of PAR (400-700 nm), $K_0(PAR)$, in different layers below the ikaite tufa surface was calculated from depth profiles of PAR calculated by integrating the measured spectra over the spectral region of interest according to Kühl (2005):

$$K_0(PAR) = -ln\frac{(E_0(PAR)_1/E_0(PAR)_2)}{z_2 - z_1} \quad (4)$$

Where $E_0(PAR)_1$ and $E_0(PAR)_2$ are the photon scalar irradiance of PAR measured at depths z_1 and z_2, respectively.

Lateral light propagation in ikaite

To evaluate the lateral light propagation in the freshly deposited ikaite matrix, we located a clean non-pigmented area in the same column-cross section used for scalar irradiance profiling. We used the same fiber-optic scalar irradiance mini probe, while the light source was substituted with a consumer grade

This article is protected by copyright. All rights reserved.

red laser pointer mounted vertically in a manually controlled micromanipulator (MM33, Märtzhäuser, Wetzlar, Germany). The diameter of the incident laser beam was measured on a 20% reflectance standard at a distance of 40 cm, i. e., the same distance as used between the laser and the ikaite for the light attenuation measurements. The laser produced a split-beam of two intersecting circles illuminating an area of ~1x2 mm with a peak emission of ~652 nm. The sensor was positioned ~9 mm into a predrilled hole in the ikaite, while measuring the spectrum of the laser light, as the laser was moved away from the light probe in lateral steps of 2 mm (Fig. 7). We calculated the average lateral light attenuation in different zones across the ikaite crystal matrix by fitting an exponential decay function to the measured data.

Accepted Article

This article is protected by copyright. All rights reserved.

Accepted Article

Acknowledgements

This study was supported by a *Sapere-Aude* Advanced grant from the Danish Council for Independent Research | Natural Sciences (MK), an Elite Researcher travel stipend from the Danish Council for Independent Research (ET), and the Carlsberg Foundation (MK). We thank professional diver and underwater photographer Jesper Kikkenborg for invaluable underwater observations and photography, as well as for excellent technical assistance in the field. Alexandra Kerbl is thanked for help and advice on staining and confocal microscopy of ikaite samples. Klaus Qvortrup and the Centre for Integrated Bioimaging are thanked for excellent assistance with SEM analysis. We thank the staff at the Danish Naval base "Flådestation Grønnedal", Greenland - in particular Simon Madsen, and John Arsuk (Ivittuut municipality) for their extraordinary logistic support and efforts to make our field trips successful. We thank the Homerule of Greenland for permission to perform research on the Ikaite columns as authorized by the Greenland Authorities under the survey license number: G13-039 (MK). The authors declare no conflict of interest.

This article is protected by copyright. All rights reserved.

Accepted Article

References

Barlow, R.G., Mantoura, R.F.C., Gough, M.A., and Fileman, T.W. (1993) Pigment signatures of the phytoplankton composition in the northeastern Atlantic during the 1990 spring bloom. Deep Sea Res Part II 40: 459–477.

Brock, T.D. (1973) Lower pH limit for the existence of blue-green algae: evolutionary and ecological implications. Science 179: 480–483.

Brooks, R., Clark, L.M., and Thurston, E.F. (1950) Calcium carbonate and its hydrates. Phil Trans Roy Soc Lond 243: 145–167.

Brunet, C., Brylinski, J.M., and Lemoine, Y. (1993) *In situ* variations of the xanthophylls diatoxanthin and diadinoxanthin: photoadaptation and relationships with a hydrodynamical system in the eastern English Channel. Mar Ecol Progr Ser 102: 69–77.

Buchardt, B., Israelson, C., Seaman, P., and Stockmann, G. (2001) Ikaite tufa towers in Ikka Fjord, Southwest Greenland: their formation by mixing of seawater and alkaline spring water. J Sed Res 71: 176–189.

Buchardt, B., Seaman, P., Stockmann, G., Vous, M., Wilken, U., Düwel, L., Kristiansen, A., Jenner, C., Whitticar, M. J., Kristensen, R. M., Petersen, G. H., and Thorbjørn, L. (1997) Submarine columns of ikaite tufa. Nature 390: 129–130.

This article is protected by copyright. All rights reserved.

Decho, A.W. (2000) Microbial biofilms in intertidal systems: an overview. Cont Shelf Res 20: 1257–1273.

Decho, A.W. (1990) Microbial exopolymer secretions in ocean environments: their role(s) in food webs and marine processes. Oceanogr Mar Biol Annu Rev 28: 73–153.

Dickens, B., and Brown, W.E. (1970) The crystal structure of calcium carbonate hexahydrate at ~-120°C. Inorg Chem 9: 480–486.

Emeleus, C. H. (1964) The Grønnedal-Ika alkaline complex, South Greenland. The structure and geological history of the complex. Medd Grønland 172: 74.

Everitt, D.A., Wright, S.W., Volkman, J.K., Thomas, D.P., and Lindstrom, E.J. (1990) Phytoplankton community compositions in the western equatorial Pacific determined from chlorophyll and carotenoid pigment distributions. Deep Sea Res A 37: 975–997.

Ezequiel, J., Laviale, M., Frankenbach, S., Cartaxana, P., and Serôdio, J. (2015) Photoacclimation state determines the photobehaviour of motile microalgae: the case of a benthic diatom. J Exp Mar Biol Ecol 468: 11–20.

Flemming, H.-C., and Wingender, J. (2010) The biofilm matrix. Nat Rev Microbiol 8: 623-633.

This article is protected by copyright. All rights reserved.

Accepted Article

Ford, T. D., and Pedley, H. M. (1996) A review of tufa and travertine deposits of the world. Earth-Sci Rev 41: 117-175.

Frigaard, N.U., Larsen, K.L., Larsen, K.L., and Cox, R.P. (1996) Spectrochromatography of photosynthetic pigments as a fingerprinting technique for microbial phototrophs. FEMS Microbiol Ecol 20: 69–77.

Garcia-Pichel, F., Mechling, M., and Castenholz, R.W. (1994) Diel migrations of microorganisms within a benthic, hypersaline mat community. Appl Environ Microbiol 60: 1500-1511.

Glaring, M.A., Vester, J.K., Lylloff, J. E. Al-Soud, W.A., Sørensen, S.J., and Stougaard, P. (2015) Microbial diversity in a permanently cold and alkaline environment in Greenland. PLoS ONE 10 (4): e0124863.

Goldman, J.C., Riley, C.B., and Dennett, M.R. (1982) The effect of pH in intensive microalgal cultures. II. Species competition. J Exp Mar Biol Ecol 57: 15–24.

Hansen, M.O., Buchardt, B., Kühl, M., and Elberling, B. (2011) The fate of the submarine ikaite tufa columns in southwest Greenland under changing climate conditions. J Sed Res 81: 553–561.

Hayat, M. A. (2000) Principles and techniques of electron microscopy: biological applications. Cambridge University Press, Cambridge, UK; New York.

This article is protected by copyright. All rights reserved.

Accepted Article

Hoff, A. J., and Amesz, J. (1991) Visible absorption spectroscopy of chlorophylls. In, Scheer, H. (ed) Chlorophylls. CRC Press, Boca Raton, pp. 723-738.

Hume, J., and Topley, B. (1926) The density of calcium carbonate hexahydrate. Chem Soc J 129: 2932–2934.

Jeffrey, S.W., Wright, S.W., and Zapata, M. (2011) Microalgal classes and their signature pigments. In, Roy,S., Llewellyn,C., Egeland,E.S., and Johnsen,G. (eds), Phytoplankton Pigments, Characterization, Chemotaxonomy and Applications in Oceanography. Cambridge University Press, Cambridge, pp. 3–77.

Johnston, J., Merwin, H.E., and Williamson, E.D. (1916) The several forms of calcium carbonate: American J Sci 41: 473–512.

Knott, G., Marchman, H., Wall, D. & Lich, B. (2008) Serial section scanning electron microscopy of adult brain tissue using focused ion beam milling. J Neurosci 28: 2959–2964.

Kristiansen, J., and Kristiansen, A. (1999) A new species of *Chroomonas* (Cryptophyceae) living inside the submarine ikaite columns in the Ikkafjord, Southwest Greenland, with remarks on its ultrastructure and ecology. Nor J Bot 19: 747–758.

This article is protected by copyright. All rights reserved.

Accepted Article

Kruschel, C. and Castenholz, R.W. (1998) The effect of solar UV and visible irradiance on the vertical movements of cyanobacteria in microbial mats. FEMS Microbiol Ecol 27: 53-72.

Kühl, M. and Polerecky, L. (2008) Functional and structural imaging of phototrophic microbial communities and symbioses. Aq Micro Ecol 53: 99–118.

Kühl, M. (2005) Optical microsensors for analysis of microbial communities. Meth Enzymol 397: 166-199.

Kühl, M., Glud, R.N., Ploug, H., and Ramsing, N.B. (1996) Microenvironmental control of photosynthesis and photosynthesis-coupled respiration in an epilithic cyanobacterial biofilm. J Phycol 32: 799-812.

Kupriyanova, E., Villarejo, A., Markelova, A., Gerasimenko, L., Zavarzin, G., Samuelsson, G., *et al.* (2007) Extracellular carbonic anhydrases of the stromatolite-forming cyanobacterium *Microcoleus chthonoplastes*. Microbiol (UK) 153: 1149–1156.

Lassen, C., Ploug, H., and Jørgensen, B.B. (1992) Microalgal photosynthesis and spectral scalar irradiance in coastal marine sediments of Limfjorden, Denmark. Limnol Oceanogr 37: 760–772.

This article is protected by copyright. All rights reserved.

Nymark, M., Valle, K.C., Hancke, K., Winge, P., Andresen, K., Johnsen, G., *et al.* (2013) Molecular and photosynthetic responses to prolonged darkness and subsequent acclimation to re-illumination in the diatom *Phaeodactylum tricornutum*. PLoS ONE 8: e58722.

Pauly, H. (1963) "Ikaite", a New Mineral from Greenland. ARCTIC 16: 263–264.

Riding, R. (2000) Microbial carbonates: the geological record of calcified bacterial-algal mats and biofilms. Sedimentol 47: 179-214.

de los Rios, A., Ascaso, C., Wierzchos, J., Vincent, W. F., and Quesada, A. (2015) Microstructure and cyanobacterial composition in microbial mats from the high Arctic. Biodiv Conserv 24: 841-863.

Roeselers, G., Norris, T.B., Castenholz, R.W., Rysgaard, S., Glud, R.N., Kühl, M., and Muyzer, G. (2007) Diversity of phototrophic bacteria in microbial mats from Arctic hot springs (Greenland). Environ Microbiol 9: 26-38.

Schmidt, M., Priemé, A., and Stougaard, P. (2006a) Bacterial diversity in permanently cold and alkaline ikaite columns from Greenland. Extremophiles 10: 551–562.

Schmidt, M., Prieme, A., and Stougaard, P. (2006b) *Rhodonellum psychrophilum* gen. nov., sp. nov., a novel psychrophilic and alkaliphilic bacterium of the phylum Bacteroidetes isolated from Greenland. Int J Syst Evol Microbiol 56: 2887–2892.

This article is protected by copyright. All rights reserved.

Accepted Article

Schmidt, M., Priemé, A., and Stougaard, P. (2007) *Arsukibacterium ikkense* gen. nov., sp. nov, a novel alkaliphilic, enzyme-producing γ-Proteobacterium isolated from a cold and alkaline environment in Greenland. Syst Appl Microbiol 30: 197–201.

Schmidt, M. and Stougaard, P. (2010a) Identification, cloning and expression of a cold‐active β‐galactosidase from a novel Arctic bacterium, *Alkalilactibacillus ikkense*. Environ Tech 31: 1107‐1114.

Schmidt, M., Larsen, D.M. and Stougaard, P. (2010b) A lipase with broad temperature range from an alkaliphilic gamma-proteobacterium isolated in Greenland. Environ Tech 31 (10): 1091-1100.

Schreiber, U., Bilger, W., and Neubauer, C. (1994) Chlorophyll fluorescence as a non-intrusive indicator for rapid assessment of *in vivo* photosynthesis. In: Schulze E-D, Caldwell MM (eds). Ecological studies, Springer, Heidelberg, pp. 49–70.

Schreiber, U. (2004) Pulse-amplitude-modulation (PAM) fluorometry and saturation pulse method: an overview. In: Papageorgiou GCG (ed) Chlorophyll fluorescence: a signature of photosynthesis. Kluwer, Dordrecht, pp. 279–319.

Seaman, P., and Buchardt, B. (2006). The columns of ikaite tufa in Ikka Fjord, Greenland. Monographs on Greenland, Geoscience 44. Copenhagen: Museum Tusculanum Press.

This article is protected by copyright. All rights reserved.

Serôdio, J., Marques da Silva, J., and Catarino, F. (1997) Nondestructive tracing of migratory rhythms of intertidal benthic microalgae using *in vivo* chlorophyll *a* fluorescence. J Phycol 33: 542–553.

Shiraishi, F., Bisset, A., de Beer, D., Reimer, A., and Arp, G. (2008) Photosynthesis, respiration and exopolymer calcium-binding in biofilm calcification (Westerhöfer and Deinschwanger Creek, Germany). Geomicrobiol J 25: pp. 83-94.

Sigernes, F., Dyland, M., Peters, N., Lorentzen, D. A., Svenøe, T., Heia, K., Chernouss, S., Deehr, C. S. And Kosch, M. (2009) The absolute sensitivity of digital color cameras. Opt. Express 17: 20211-20220.

Singh, S.M., and Elster, J. (2007) Cyanobacteria in Antarctic lake environments. In: Algae and Cyanobacteria in Extreme Environments, Cellular Origin, Life in Extreme Habitats and Astrobiology Vol. 11, Springer Netherlands: Dordrecht, pp. 303–320.

Smith, H.D., McKay, C.P., Duncan, A.G., Sims, R.C., Anderson, A.J., and Grossl, P.R. (2014) An instrument design for non-contact detection of biomolecules and minerals on Mars using fluorescence. J Biol Engin 8:16.

Stambler, N. and Dubinsky, Z. (2007) Marine phototrophs in the twilight zone. In, Seckbach,J. (ed), *Algae and Cyanobacteria in Extreme Environments*, Cellular Origin, Life in Extreme Habitats and Astrobiology. Springer Netherlands, Dordrecht, pp. 79–97.

This article is protected by copyright. All rights reserved.

Accepted Article

Stougaard, P., Jørgensen, F., Johnsen, M.G., and Hansen, O.C. (2002) Microbial diversity in ikaite tufa columns: an alkaline, cold ecological niche in Greenland. Environ Microbiol 4: 487-493.

Stuart, R. K., Mayali, X., Lee, J. Z., Craig Everroad, R., Hwang, M., Bebout, B. M., *et al.* (2016). Cyanobacterial reuse of extracellular organic carbon in microbial mats. ISME J 10: 1240–1251.

Tashyreva, D. and Elster, J. (2016) Annual cycles of two cyanobacterial mat communities in hydro-terrestrial habitats of the high Arctic. Microb Ecol 71: 887–900.

Taylor, J.D., McKew, B.A., Kuhl, A., McGenity, T.J., and Underwood, G.J.C. (2013) Microphytobenthic extracellular polymeric substances (EPS) in intertidal sediments fuel both generalist and specialist EPS-degrading bacteria. Limnol Oceanogr 58: 1463–1480.

Trampe. E., Kolbowski, J., Schreiber, U., and Kühl, M. (2011) Rapid assessment of different oxygenic phototrophs and single-cell photosynthesis with multicolour variable chlorophyll fluorescence imaging. Mar Biol 158:1667–1675.

Trampe, E., Larsen, J.E.N., Glaring, M.A., Stougaard, P., and Kühl, M. (2016) *In situ* dynamics of O_2, pH, light and photosynthesis in ikaite tufa columns (Ikka Fjord, Greenland) – a unique microbial habitat. Front Microbiol 7: 722.

Vester, J.K., Lylloff, J.E., Glaring, M.A., and Stougaard, P. (2013) Microbial diversity and enzymes in Ikaite columns: a cold and alkaline environment in Greenland. In, Seckbach,J. (ed), *Algae and*

This article is protected by copyright. All rights reserved.

Accepted Article

Cyanobacteria in Extreme Environments, Cellular Origin, Life in Extreme Habitats and Astrobiology. Springer Netherlands, Dordrecht, 365–380.

Vester, J.K., Glaring, M.A., and Stougaard, P. (2014) Discovery of novel enzymes with industrial potential from a cold and alkaline environment by a combination of functional metagenomics and culturing. Microb Cell Fact 13: 72.

Vincent, W.F., Castenholz, R.W., Downes, M.T., and Howard Williams, C. (1993) Antarctic cyanobacteria: light, nutrients, and photosynthesis in the microbial mat environment. J Phycol 29: 745–755.

Wangpraseurt, D., Larkum, A. W. D., Franklin, J., Szabo, M., Ralph, P. J, and Kühl, M. (2014) Lateral light transfer ensures efficient resource distribution in symbiont-bearing corals. J Exp Biol 217: 489-498.

Webb, W.L., Newton, M., and Starr, D. (1974) Carbon dioxide exchange of *Alnus rubra*. Oecologia 17: 281–291.

Wieland, A. and Kühl, M. (2000) Irradiance and temperature regulation of oxygenic photosynthesis and O_2 consumption in a hypersaline cyanobacterial mat (Solar Lake, Egypt). Mar Biol 137: 71–85.

This article is protected by copyright. All rights reserved.

Zapata, M., Rodríguez, F., and Garrido, J.L. (2000) Separation of chlorophylls and carotenoids from marine phytoplankton: a new HPLC method using a reversed phase C8 column and pyridine-containing mobile phases. Mar Ecol Progr Ser 195: 29-45.

Accepted Article

This article is protected by copyright. All rights reserved.

Accepted Article

Figure Legends

Figure 1

Ikaite tufa columns harboring microbial phototrophs. (A) Underwater photo of tufa columns in Ikka Fjord, Greenland; background shows diver-operated microsensor measurements. (B) Micrograph of ikaite crystals in a tufa column sample. Micrographs of ikaite crystal matrix colonized by cyanobacteria (C), and diatoms (D). Scale bars represent 200 μm.

Figure 2

Color-coded confocal laser scanning micrograph of an ikaite sample showing the presence of TRITC-labeled Lectin-stained exopolymers (A, yellow; ex./em. 488/500-550 nm), autofluorescence of cyanobacteria (B, orange-red; ex./em. 543/585-625 nm) and diatoms (C, red; ex./em. 635/650-800 nm), DAPI-stained bacterial cells (D, blue; ex./em. 405/461 nm), and calcein-stained ikaite crystals (E, black, shown as surface based on data obtained by recording of transmitted light images and calcein-staining (ex./em. 633/650 nm). Scale bar represents 30 μm.

Figure 3

Scanning electron micrographs of ikaite sample with certain structures enhanced in false colors. (A) Overview image with ikaite crystals shown in light blue, filamentous cyanobacteria in green, non-phototrophic bacterial cells in yellow, and amorphous collapsed exopolymeric material (EPS) in grey. (B) Close-up image showing a cyanobacterial filament with an enlarged heterocyst, and partly covered with heterotrophic bacteria (yellow) and EPS.

This article is protected by copyright. All rights reserved.

Figure 4

Macroscopic fluorescence imaging of a longitudinal cross-section through the apex of an ikaite column. (A) Cyan color indicates fluorescence from cyanobacterial phycobiliproteins (phycoerythrin) when excited by green light (515-560 nm). (B) Red color indicates fluorescence from diatoms when exited by blue light (450-492 nm). (C) Color photograph of the ikaite column apex. (D) Superimposed images of panel A and B. Scale bars represent 2 cm.

Figure 5

HPLC chromatogram (absorbance at 430 nm vs. retention time of sample fractions) of a bulk ikaite sample extract, showing photopigment composition in the outermost 3 cm of an ikaite column. Assignment of pigments to individual peaks were based on absorbance spectra of the respective sample fractions as listed in Table 1.

Figure 6

Light penetration in ikaite. (A) Overview of spectral scalar irradiance measurements performed in the ikaite matrix of a horizontal cross section from a column apex sample. Series # 1, 2, and 3 indicate the displayed measuring points. The direction of incident light during measurements is indicated by the yellow arrow. The shaft of the light probe is visible in the third hole in series #1. (B) Spectral scalar irradiance at increasing depth inside the ikaite matrix. The spectra represent averages of 3 measurements in each depth interval (noted on each curve in the graph). Measurements were normalized to the incident collimated irradiance at the column surface, measured without the sample in the measurement chamber. Absorption ranges of predominant photopigments causing minima in the transmittance spectra are highlighted in grey. (C) Depth profile of photon scalar irradiance (PAR, 400-

This article is protected by copyright. All rights reserved.

Accepted Article

700 nm) showing the light attenuation in the ikaite matrix with increasing depth from the tufa column surface. Dotted lines with different slopes indicate layers with different scalar irradiance attenuation coefficients.

Figure 7

Scattering and lateral light attenuation in hydrated clean ikaite. (A) Scattering and lateral light propagation in ikaite (laser beam point- red mark in lower left). Overview of lateral light attenuation measurements, probe inserted in a predrilled hole of a ikaite tufa cross section at a distance from a focused laser light, consecutive holes were drilled, and light measured at decreasing distance from the laser point. (B) Spectral scalar irradiance of red laser light measured at different lateral distances between the light sensor and the incident laser beam; dashed lines indicate the range over which the spectra were integrated. (C) Lateral light attenuation of red light (647-658 nm) measured at increasing lateral distance to the incident laser beam (in % of incident light directly in the beam). The data were fitted with a mono-exponential decay function (r^2 >0.985).

Figure 8

Photosynthesis in an ikaite sample with endolithic phototrophs assessed by macroscopic variable chlorophyll fluorescence imaging. (A-B) Rapid light curves showing the relative electron transport rate (rETR), and effective PSII quantum yield (Φ_{PSII}) as a function of increasing photon irradiance measured at three different locations on an ikaite column cross section. (C) Digital photograph showing ikaite cross-section with endolithic biofilm. (D) Maximal fluorescence image mapping the fluorescence intensity image in false colors according to the color scale bar. Numbered circles indicate areas of

This article is protected by copyright. All rights reserved.

interest for averaging of data presented in panels A and B. (E) Display of maximal PS II quantum yield of dark adapted phototrophs in false color according to the color scale bar.

Figure 9

Photosynthesis of individual endolithic cyanobacteria and diatoms assessed by microscopic variable chlorophyll fluorescence imaging. (A-B) Rapid light curves show the relative electron transport rate (rETR) and effective PSII quantum yield (Φ_{PSII}) as a function of increasing photon irradiance in the ikaite matrix. (C) Deconvoluted image showing in false colors the main functional phototrophic groups, cyanobacteria in blue, and diatoms in yellow inside the ikaite matrix. (D) Maximal fluorescence image mapping the fluorescence intensity image in false colors according to the color scale bar. (E) Image of maximal PS II quantum yield of dark-adapted phototrophs in false color according to the color scale bar. Symbols with error bars represent means ± SE (n= 17 diatom cells and n= 13 cyanobacterial filaments).

Figure 10

Schematic drawing of the apex of an ikaite column, harboring an endolithic community of cyanobacteria (green) and diatoms (yellow) in the ikaite crystal matrix. Arrows show direction of alkaline (pH 10) ikaite water flow, where the large arrow indicate the water flow in a flow-channel, and small arrows indicate the more diffuse flow of pore water through the outermost ikaite layers, where fresh deposition occurs in a mixing zone with seawater (indicated by spheres). Physico-chemical gradients across the ikaite column are indicated at the base of the figure with color scale bars, where the O_2 gradient shown represents photosynthetic O_2 evolution during daylight in summer.

This article is protected by copyright. All rights reserved.

Accepted Article

Accepted Article

Supp. Fig. 1

Video sequence showing a spatial representation of rendered confocal image stacks recorded in a fresh ikaite sample. (A) Yellow resembles EPS staining, (B) autofluorescence of filamentous cyanobacteria, (C) autofluorescence of diatoms, (D) heterotrophs, (E) Black resembles $CaCO_3$ staining. Scale bar represents 30 μm.

Supp. Fig. 2

Digital microscopy video of EPS binding of a diatom dominated biofilm and ikaite crystals.

Supp. Fig. 3

Underwater time-lapse video, the 20 s video is showing a 6 min long observation, speed 18X, of an ikaite column apex grazed on by numerous sea urchins. Notice the whitish fecal pellets (presumably ikaite) being released from the aboral side of the urchins.

This article is protected by copyright. All rights reserved.

Accepted Article

Table 1

Pigments detected by HPLC analysis in the outermost 3 cm of an ikaite column. Peak numbers, elution times, and spectrographic absorbance maxima are noted, while wavelengths in brackets denote characteristic shoulders in the spectra.

Peak #	Pigment	Retention time (min)	Visible absorbance spectra (nm)		
1	Fucoxanthin	11.89	454		
2	Unknown	13.74	(450)	482	508
3	Diadinoxanthin	17.33	(424)	448	478
4	Zeaxanthin	20.56	(430)	452	480
5	Unknown carotenoid	23.65	(422)	446	475
6	Unknown carotenoid	26.45	(422)	447	476
7	Unknown carotenoid	28.07	(422)	446	475
8	Unknown	30.69		473	
9	BChl *a*	40.76	365	603	771
10	Chlorophyll *b*	42.42	462	598	648
11	β,ε-carotene	43.15	(422)	448	675
12	Chlorophyll *a*	47.76	431	616	664
13	Phaeophytin *a*	55.24	409	609	666
14	Unknown	56.87	(426)	455	485
15	Unknown carotenoid	57.35	(434)	462	492
16	Unknown carotenoid	58.75	(422)	447	475
17	Unknown carotenoid	59.53	(422)	447	475
18	Phaeophytin *a*	60.16	409	609	666

This article is protected by copyright. All rights reserved.

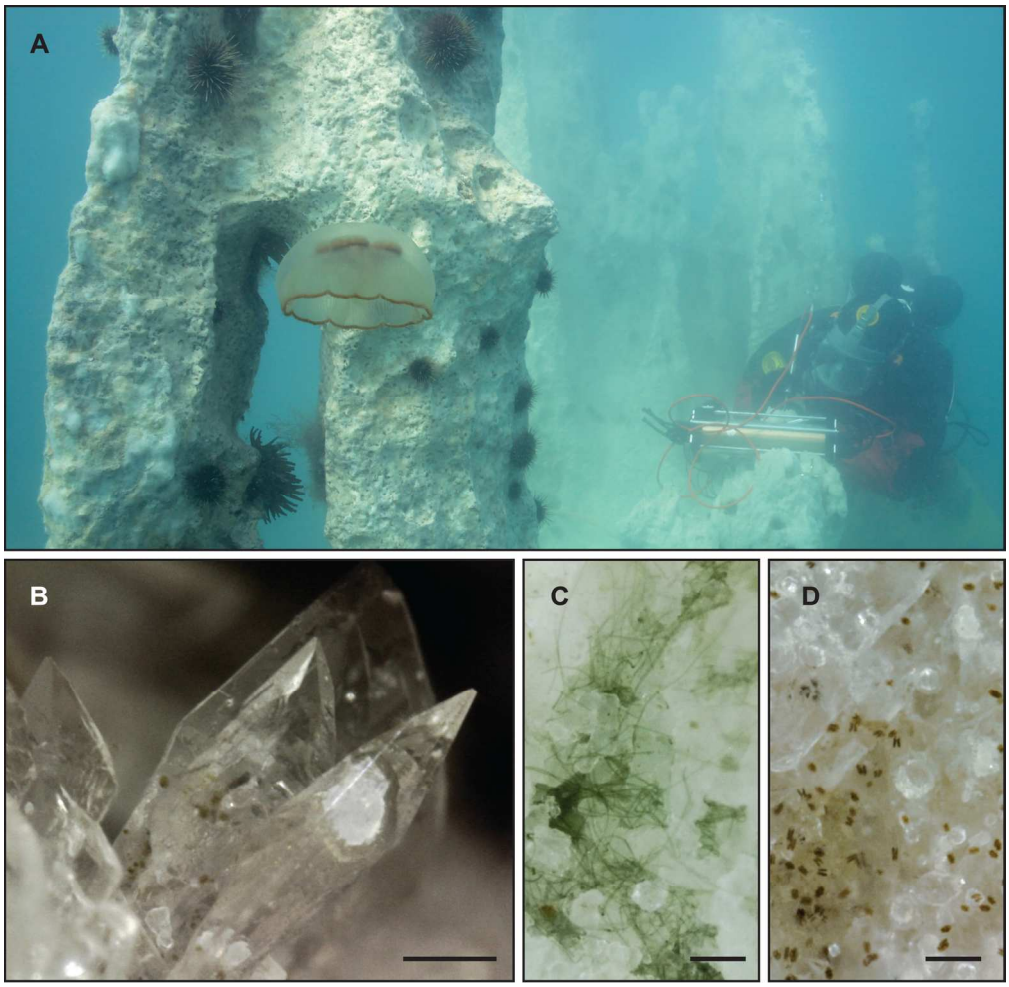

Figure 1
Ikaite tufa columns harboring microbial phototrophs. (A) Underwater photo of tufa columns in Ikka Fjord, Greenland; background shows diver-operated microsensor measurements. (B) Micrograph of ikaite crystals in a tufa column sample. Micrographs of ikaite crystal matrix colonized by cyanobacteria (C), and diatoms (D). Scale bars represent 200 µm.

155x151mm (300 x 300 DPI)

Acc

This article is protected by copyright. All rights reserved.

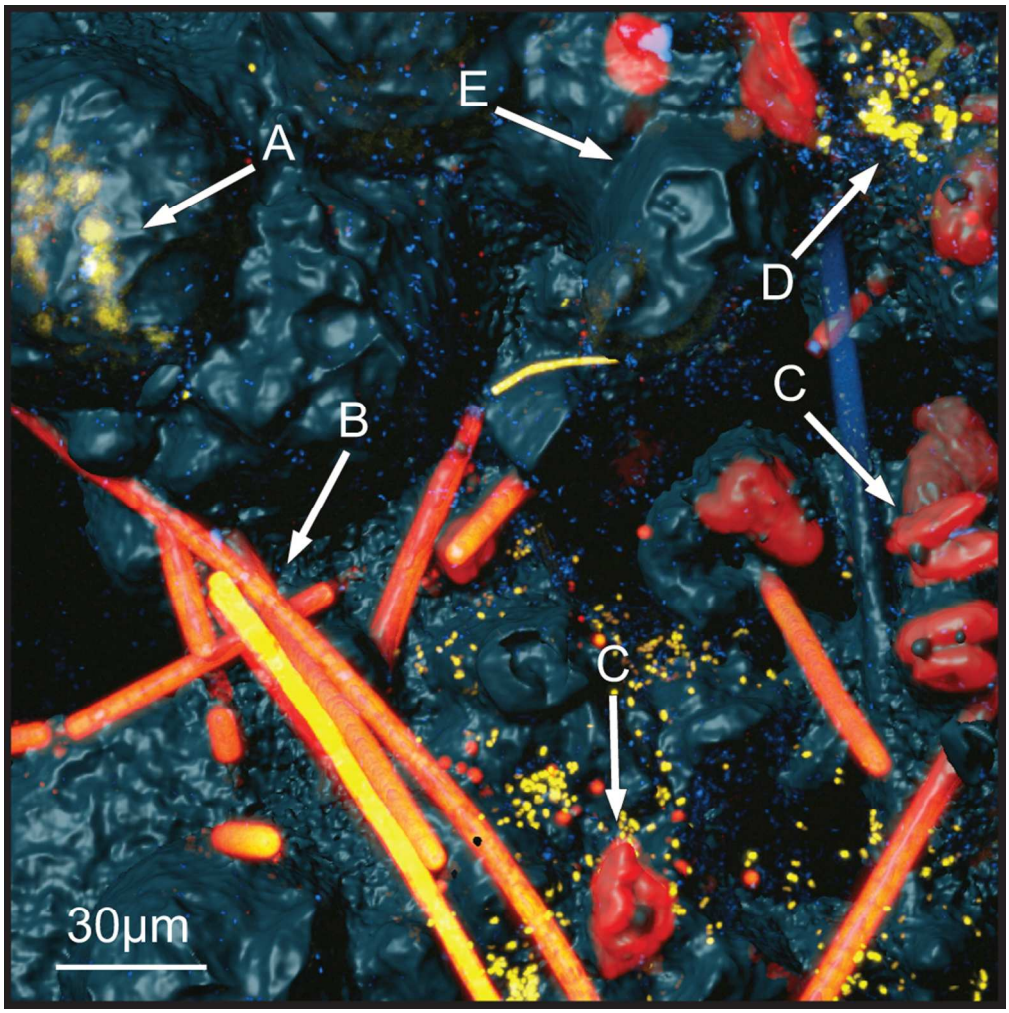

Color-coded confocal laser scanning micrograph of an ikaite sample showing the presence of TRITC-labeled Lectin-stained exopolymers (A, yellow; ex./em. 488/500-550 nm), autofluorescence of cyanobacteria (B, orange-red; ex./em. 543/585-625 nm) and diatoms (C, red; ex./em. 635/650-800 nm), DAPI-stained bacterial cells (D, blue; ex./em. 405/461 nm), and calcein-stained ikaite crystals (E, black, shown as surface based on data obtained by recording of transmitted light images and calcein-staining (ex./em. 633/650 nm). Scale bar represents 30 µm.

86x86mm (300 x 300 DPI)

Wiley-Blackwell and Society for Applied Microbiology

This article is protected by copyright. All rights reserved.

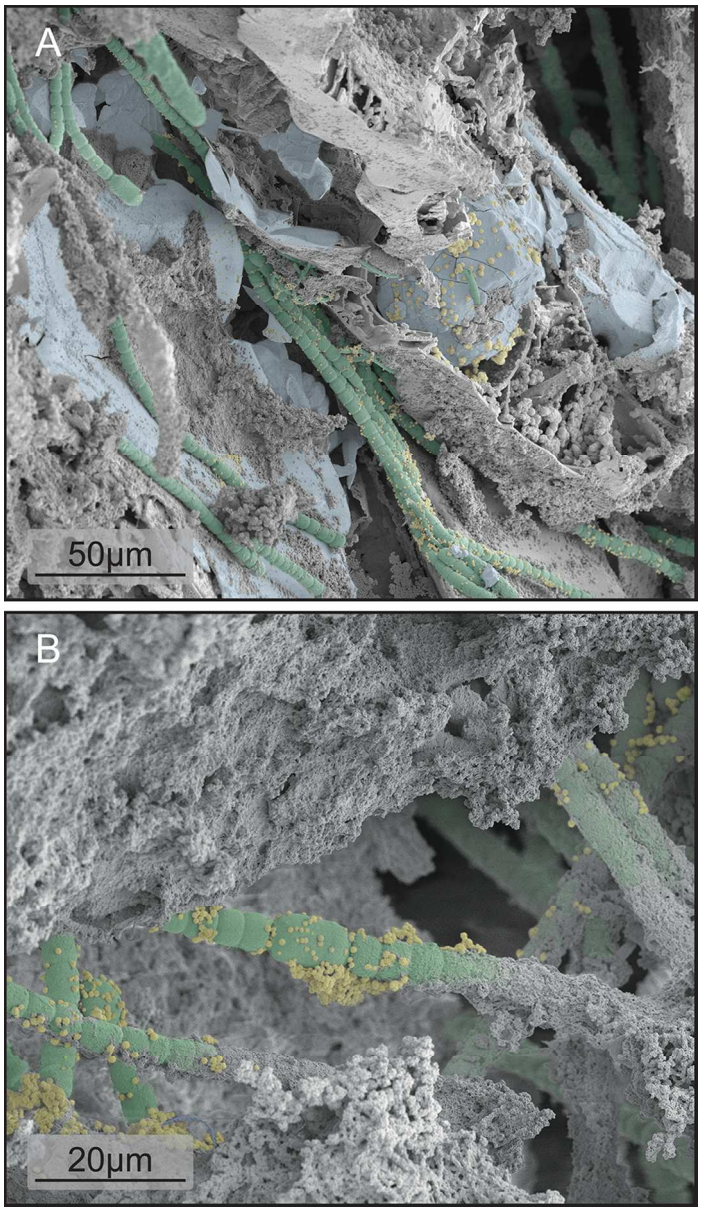

Figure 3‼ ┼
Scanning electron micrographs of ikaite sample with certain structures enhanced in false colors. (A) Overview image with ikaite crystals shown in light blue, filamentous cyanobacteria in green, non-phototrophic bacterial cells in yellow, and amorphous collapsed exopolymeric material (EPS) in grey. (B) Close-up image showing a cyanobacterial filament with an enlarged heterocyst and partly covered with heterotrophic bacteria (yellow) and EPS.

86x150mm (300 x 300 DPI)

This article is protected by copyright. All rights reserved.

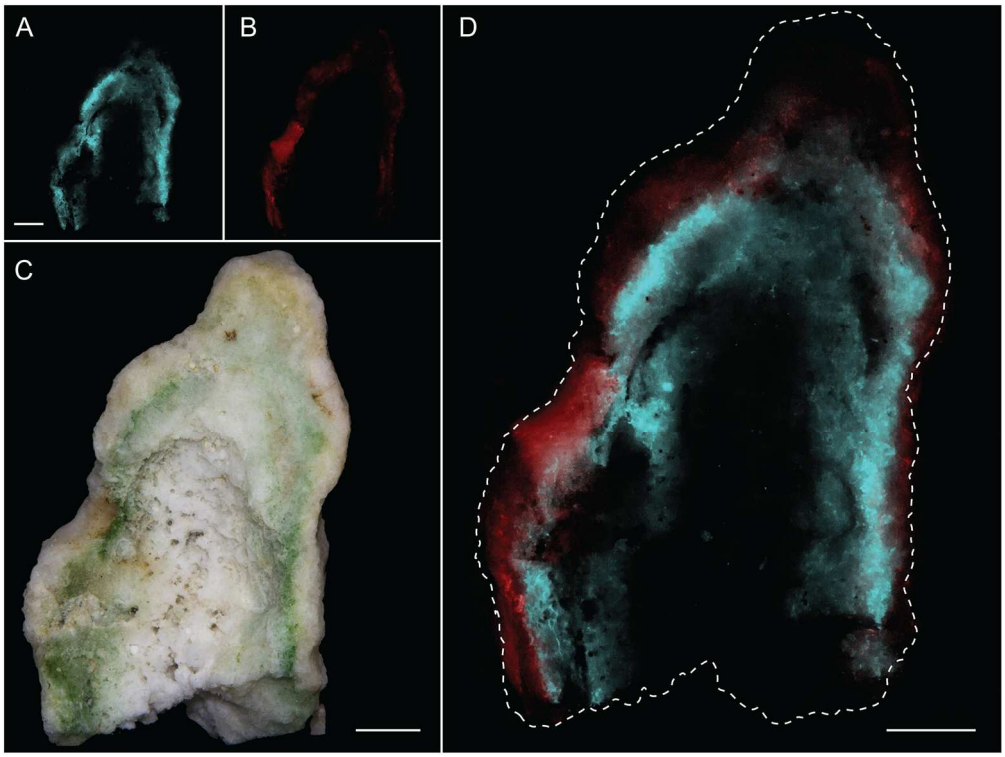

Macroscopic fluorescence imaging of a longitudinal cross-section through the apex of an ikaite column. (A) Cyan color indicates fluorescence from cyanobacterial phycobiliproteins (phycoerythrin) when excited by green light (515-560 nm). (B) Red color indicates fluorescence from diatoms when exited by blue light (450-492 nm). (C) Color photograph of the ikaite column apex. (D) Superimposed images of panel A and B. Scale bars represent 2 cm.

158x119mm (300 x 300 DPI)

Accept

This article is protected by copyright. All rights reserved.

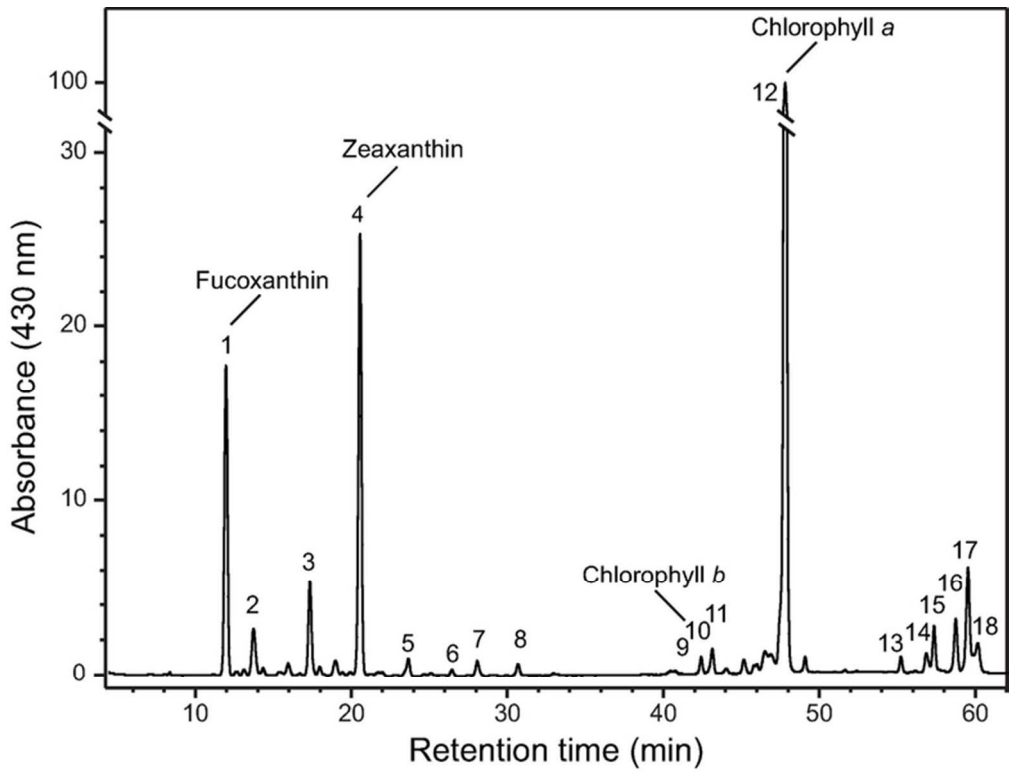

HPLC chromatogram (absorbance at 430 nm vs. retention time of sample fractions) of a bulk ikaite sample extract, showing photopigment composition in the outermost 3 cm of an ikaite column. Assignment of pigments to individual peaks were based on absorbance spectra of the respective sample fractions as listed in Table 1.

65x50mm (300 x 300 DPI)

Accep

This article is protected by copyright. All rights reserved.

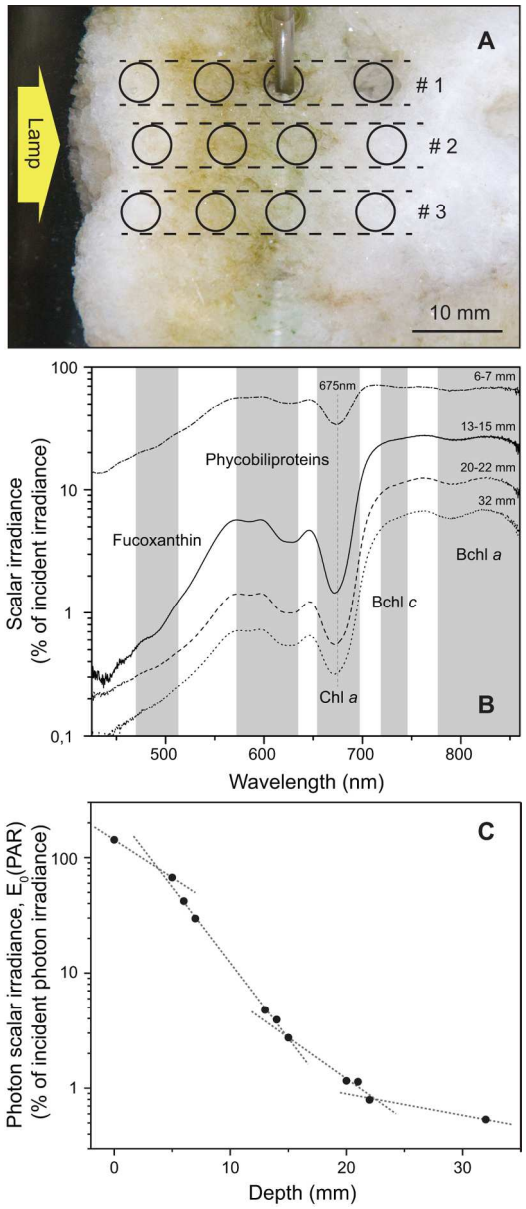

Light penetration in ikaite. (A) Overview of spectral scalar irradiance measurements performed in the ikaite matrix of a horizontal cross section from a column apex sample. Series # 1, 2 and 3, indicate the displayed measuring points. The direction of incident light during measurements is indicated by the yellow arrow. The shaft of the light probe is visible in the third hole in series #1. (B) Spectral scalar irradiance at increasing depth inside the ikaite matrix. The spectra represent averages of 3 measurements in each depth interval (noted on each curve in the graph). Measurements were normalized to the incident collimated irradiance at the column surface, measured without the sample in the measurement chamber. Absorption ranges of predominant photopigments causing minima in the transmittance spectra are highlighted in grey. (C) Depth profile of photon scalar irradiance (PAR, 400-700 nm) showing the light attenuation in the ikaite matrix with increasing depth from the tufa column surface. Dotted lines with different slopes indicate layers with different scalar irradiance attenuation coefficients.

89x206mm (300 x 300 DPI)

This article is protected by copyright. All rights reserved.

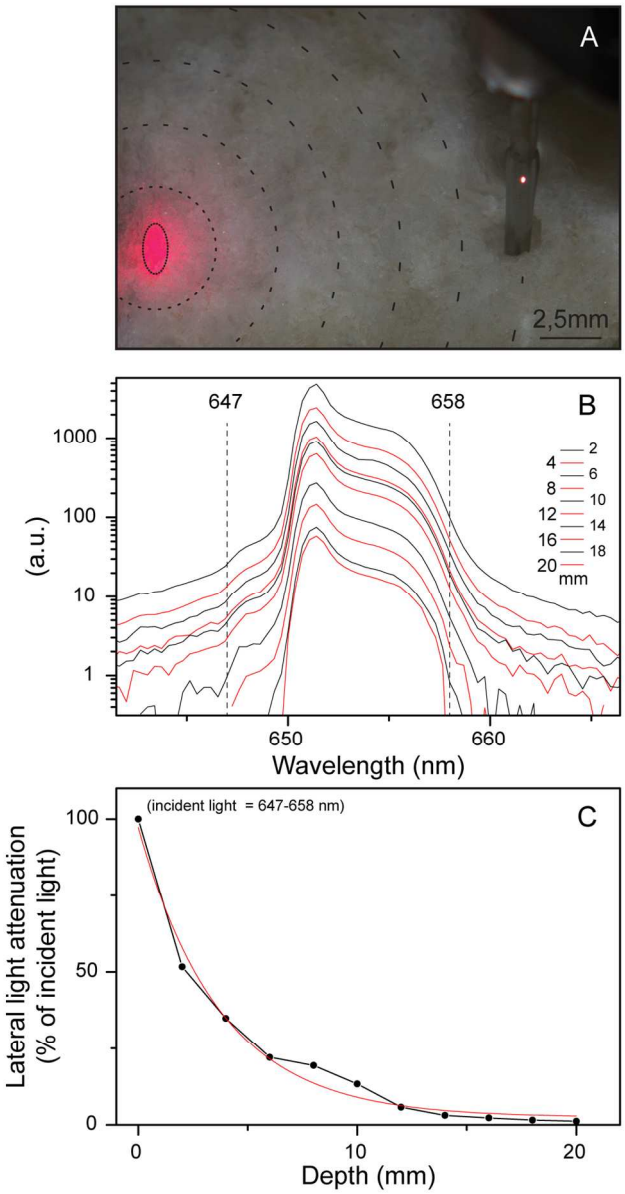

Scattering and lateral light attenuation in hydrated clean ikaite. (A) Scattering and lateral light propagation in ikaite (laser beam point- red mark in lower left). Overview of lateral light attenuation measurements, probe inserted in a predrilled hole of a ikaite tufa cross section at a distance from a focused laser light, consecutive holes were drilled and light measured at decreasing distance from the laser point. (B) Spectral scalar irradiance of red laser light measured at different lateral distances between the light sensor and the incident laser beam; dashed lines indicate the range over which the spectra were integrated. (C) Lateral light attenuation of red light (647-658 nm) measured at increasing lateral distance to the incident laser beam (in % of incident light directly in the beam). The data were fitted with a mono-exponential decay function (r2 >0.985).

88x166mm (300 x 300 DPI)

This article is protected by copyright. All rights reserved.

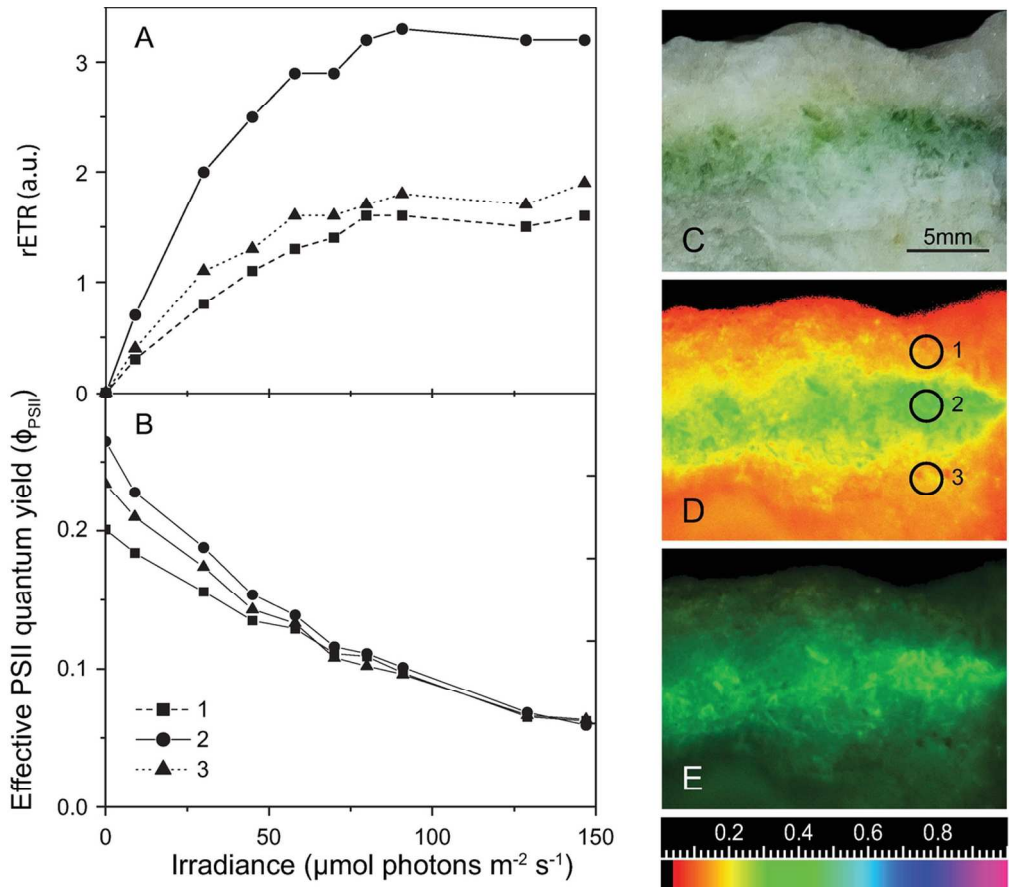

Photosynthesis in an ikaite sample with endolithic phototrophs assessed by macroscopic variable chlorophyll fluorescence imaging. (A-B) Rapid light curves showing the relative electron transport rate (rETR), and effective PSII quantum yield (ΦPSII) as a function of increasing photon irradiance measured at three different locations on an ikaite column cross section. (C) Digital photograph showing ikaite cross-section with endolithic biofilm. (D) Maximal fluorescence image mapping the fluorescence intensity image in false colors according to the color scale bar. Numbered circles indicate areas of interest for averaging of data presented in panels A and B. (E) Display of maximal PS II quantum yield of dark adapted phototrophs in false color according to the color scale bar.

110x97mm (300 x 300 DPI)

Acc

This article is protected by copyright. All rights reserved.

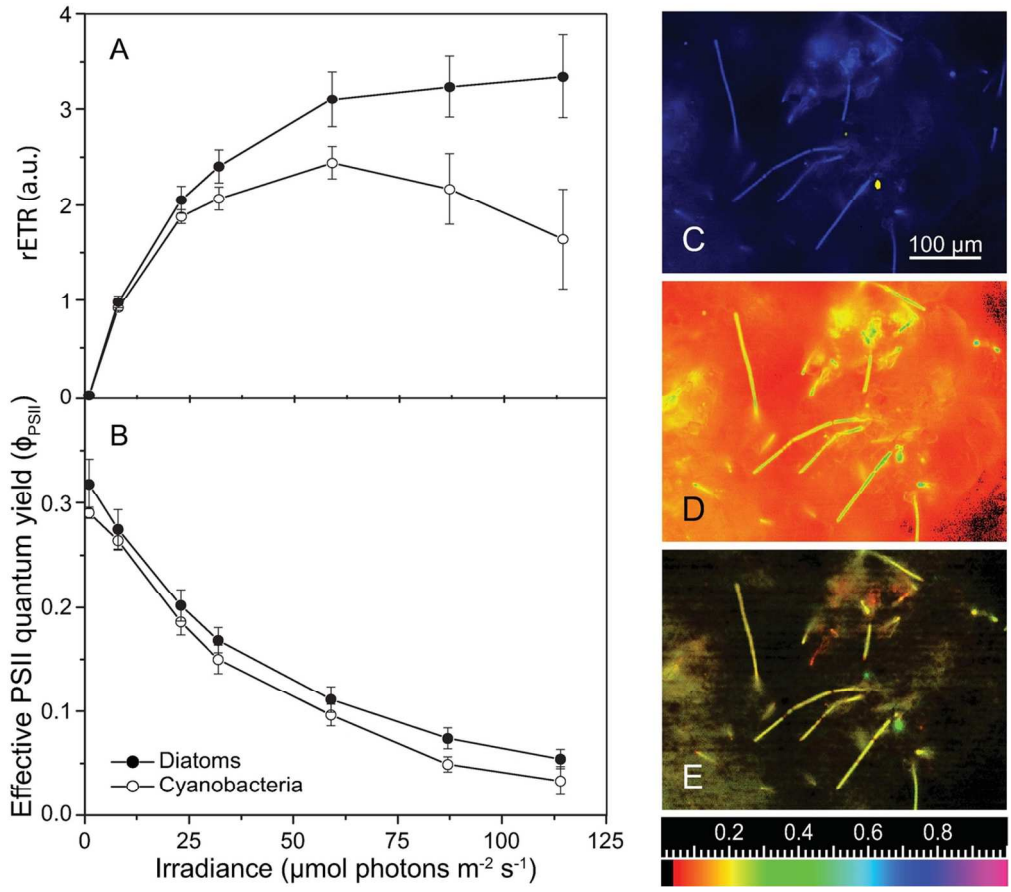

Photosynthesis of individual endolithic cyanobacteria and diatoms assessed by microscopic variable chlorophyll fluorescence imaging. (A-B) Rapid light curves show the relative electron transport rate (rETR) and effective PSII quantum yield (ΦPSII) as a function of increasing photon irradiance in the ikaite matrix. (C) Deconvoluted image showing in false colors the main functional phototrophic groups, cyanobacteria in blue, and diatoms in yellow inside the ikaite matrix. (D) Maximal fluorescence image mapping the fluorescence intensity image in false colors according to the color scale bar. (E) Image of maximal PS II quantum yield of dark-adapted phototrophs in false color according to the color scale bar. Symbols with error bars represent means ± SE (n= 17 diatom cells and n= 13 cyanobacterial filaments).

111x97mm (300 x 300 DPI)

Acc

This article is protected by copyright. All rights reserved.

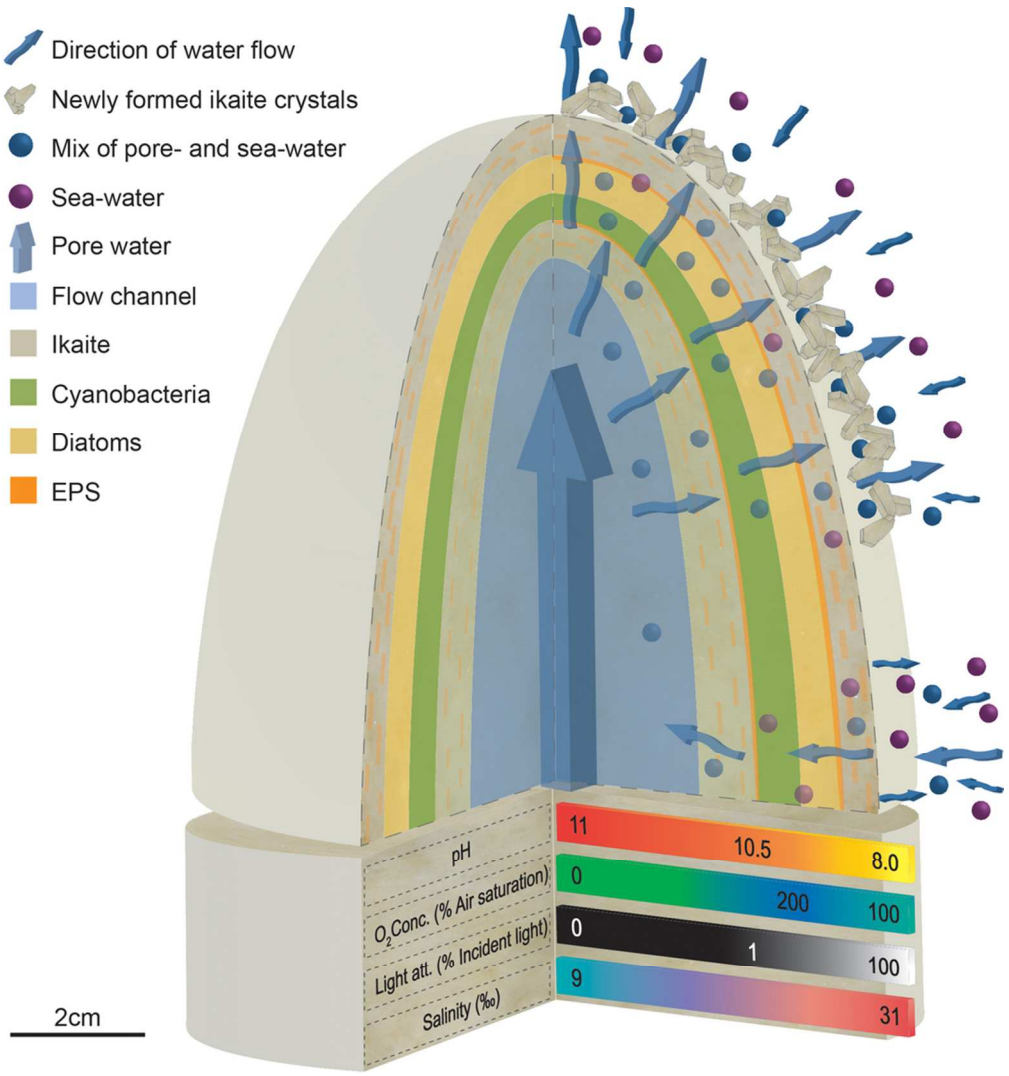

Schematic drawing of the apex of an ikaite column, harboring an endolithic community of cyanobacteria (green) and diatoms (yellow) in the ikaite crystal matrix. Arrows show direction of alkaline (pH 10) ikaite water flow, where the large arrow indicate the water flow in a flow-channel and small arrows indicate the more diffuse flow of pore water through the outermost ikaite layers, where fresh deposition occurs in a mixing zone with seawater (indicated by spheres). Physico-chemical gradients across the ikaite column are indicated at the base of the figure with color scale bars, where the O2 gradient shown represents photosynthetic O2 evolution during daylight in summer.

91x96mm (300 x 300 DPI)

Wiley-Blackwell and Society for Applied Microbiology

This article is protected by copyright. All rights reserved.